Title

Predicted constrained accessible regions mark regulatory elements and causal variants

Kohei Tomizuka[1]†, Masaru Koido[1,2]†,*, Akari Suzuki[3]†, Soichiro Yoshino[1], Nao Tanaka[1], Yuki Ishikawa[1], Xiaoxi Liu[1], Satoshi Koyama[4], Kazuyoshi Ishigaki[5], Yasuhiro Murakawa[6], Immune transcript/enhancer consortium (ITEC)[#], Kazuhiko Yamamoto[3,7], Chikashi Terao[1,8,9,*]

Affiliations

[1]Laboratory for Statistical and Translational Genetics, RIKEN Center for Integrative Medical Sciences, 1-7-22 Suehiro-cho, Tsurumi-ku, Yokohama City, Kanagawa, 230-0045, Japan.

[2]Laboratory of Complex Trait Genomics, Department of Computational Biology and Medical Sciences, Graduate School of Frontier Sciences, The University of Tokyo, 4-6-1, Shirokane-dai, Minato-ku, Tokyo, 108-8639, Japan.

[3]Laboratory for Autoimmune Diseases, RIKEN Center for Integrative Medical Sciences, 1-7-22 Suehiro-cho, Tsurumi-ku, Yokohama City, Kanagawa, 230-0045, Japan.

[4]Laboratory for Cardiovascular Genomics and Informatics, RIKEN Center for Integrative Medical Sciences, 1-7-22 Suehiro-cho, Tsurumi-ku, Yokohama City, Kanagawa, 230-0045, Japan.

[5]Laboratory for Human Immunogenetics, RIKEN Center for Integrative Medical Sciences, 1-7-22 Suehiro-cho, Tsurumi-ku, Yokohama City, Kanagawa, 230-0045, Japan.

[6]RIKEN-IFOM Joint Laboratory for Cancer Genomics, RIKEN Center for Integrative Medical Sciences, 1-7-22 Suehiro-cho, Tsurumi-ku, Yokohama City, Kanagawa, 230-0045, Japan.

[7]Drug Discovery Antibody Platform Unit, RIKEN Center for Integrative Medical Sciences, 1-7-22 Suehiro-cho, Tsurumi-ku, Yokohama City, Kanagawa, 230-0045, Japan.

[8]Clinical Research Center, Shizuoka General Hospital, 4 Chome-27-1 Kitaando, Aoi Ward, Shizuoka, 420-8527, Japan.

[9]Department of Applied Genetics, The School of Pharmaceutical Sciences, University of Shizuoka, 52-1 Yada, Suruga Ward, Shizuoka, 422-8526, Japan.

[#]Immune transcript/enhancer consortium (ITEC) members

Matteo Guerrini, Hiroaki Hatano, Keiko Hikino, Kazuyoshi Ishigaki, Yuki Ishikawa, Michihiro Kono, Xiaoxi Liu, Yasuhiro Murakawa, Masahiro Nakano, Akiko Oguchi, Raku Son, Akari Suzuki, Kazuhiro Takeuchi, Nao Tanaka, Chikashi Terao, Kohei Tomizuka, Kazuhiko Yamamoto, Soichiro Yoshino

†These authors contributed equally: Kohei Tomizuka, Masaru Koido, Akari Suzuki

*Corresponding authors:

Chikashi Terao (chikashi.terao@riken.jp)

Masaru Koido (masaru.koido@a.riken.jp)

Abstract

Open chromatin regions (OCRs) provide genome-wide DNA elements in a cell-type-specific manner at high resolution but do not always mark active regulatory regions, hampering pinpointing causal functional variants in genetic association studies. Here, we developed a new scoring system, CAMBUS (Chromatin Accessibility Mutation Burden Score), to find active and constraint OCRs via machine-learning predictions of OCRs from surrounding DNA sequences. CAMBUS predicted 66,043 active and constrained OCRs in 29 immune cell types. These OCRs were highly constrained and enriched in known

enhancers and super-enhancers. By exploiting the resolution of OCRs, we identified regulatory elements overlapping with known regulatory pathogenic variants of immune-mediated diseases and experimentally-proven or putative causal variants of complex traits, especially leukocyte-related traits, even for rare variants. In summary, our approach can derive hidden constrained and functional OCRs in a cell-type-dependent manner, thus informing non-coding causal genetic factors to human diseases at high resolution.

Introduction

Genome-wide association studies (GWAS) have identified thousands of variants significantly associated with human complex traits. However, the identification of causal variants and genes is still challenging (Maurano, Humbert et al. 2012, Visscher, Wray et al. 2017, Schaid, Chen et al. 2018). Most genetic variants (~90%) associated with complex traits in GWAS are in non-coding regions (Maurano, Humbert et al. 2012, Claussnitzer, Cho et al. 2020), especially active regulatory regions (Trynka, Sandor et al. 2013, Soskic, Cano-Gamez et al. 2019). Active regulatory elements, such as enhancers, specify cell identity, depending on cell type and cellular state (Andersson, Gebhard et al. 2014, Soskic, Cano-Gamez et al. 2019, Gupta, Weinand et al. 2023). There are several methods to identify candidate regulatory regions at a whole-genome scale: Chromatin Immuno-Precipitation sequencing (ChIP-seq) of histone modifications, DNase I hypersensitive sites sequencing (DNase-seq), and Assay for transposase-accessible chromatin using sequencing (ATAC-seq). ATAC-seq has recently been widely used to identify OCRs due to the simplicity of experimental procedures and the robustness of identified OCRs (Buenrostro, Giresi et al. 2013, Yan, Powell et al. 2020). OCRs from ATAC-seq show high positional specificity to identify regulatory elements compared with peaks from ChIP-seq (Consortium, Moore et al.

2020). Since open chromatin is a crucial state in regulating gene transcription, mapping non-coding GWAS variants to relevant OCRs has contributed to interpreting the variants' functions (Zeng, Bendl et al. 2024); however, distinguishing active regulatory regions from OCRs is still challenging since ATAC-seq does not directly measure the activity of regulatory regions (Thibodeau, Uyar et al. 2018, Klemm, Shipony et al. 2019). Therefore, additional efforts to characterize the OCRs' activity have deepened our understanding of the role of GWAS causal variants in transcriptional regulation.

Combining ATAC-seq with functional elements measured by other technologies can characterize the functions of OCRs. For example, the Encyclopedia of DNA Elements (ENCODE) consortium phase 3 used the strength of ChIP-seq signals for histone marks (H3K4me3 and H3K27ac) and CCCTC-binding factor (CTCF). It classified about 2.2 million OCRs into several groups (*e.g.*, proximal enhancer-like elements), identifying about one million candidate cis-regulatory elements (cCREs). GWAS significant variants are highly enriched in cCREs in the human genome (Consortium, Moore et al. 2020). Further incorporating interactions between regulatory elements will lead to pinpointing or narrowing down pairs of causal genes and GWAS causal variants in complex traits, as shown in studies about the activity-by-contact (ABC) model, which integrates cell-type-specific activity from histone mark ChIP-seq and contact map measured by Hi-C (Nasser, Bergman et al. 2021). Another approach for characterizing OCRs is focusing on constraint regions. GWAS causal variants tend to be located in primate- or mammalian-specific constraint regions (Andrews, Fan et al. 2023, Kuderna, Ulirsch et al. 2024), and also non-coding constraint regions defined with 76,156 human genomes (Chen, Francioli et al. 2024). Since the construction of comprehensive maps of constrained regulatory regions across cell types is still challenging, these previous findings indicate that identifying constrained and cell-type-specific (active) regulatory elements should accelerate the identification and interpretation of GWAS causal variants.

Genetic variants that change peaks in OCRs are useful for interpreting the roles of GWAS causal variants. Chromatin accessibility quantitative trait loci (caQTLs), identified from read counts from ATAC-seq on multiple individuals, are overlapped with many GWAS variants (Kumasaka, Knights et al. 2016, Gate, Cheng et al. 2018), and altering chromatin openness is thought as one of the functions of causal variants. Thus, a landscape of genetic variants affecting chromatin openness across various cell types would inform us of the unknown basis of constrained genomes and causal variants of complex traits.

While QTLs require hundreds of subjects and are not good at evaluating rare variants, machine learning can learn the basics of genetic components underlying functional elements via DNA sequences and predict the elements genome-wide. Furthermore, models based on machine learning enable us to infer variants' effects (not associations) on functional elements (Zhou, Theesfeld et al. 2018, Eraslan, Avsec et al. 2019, Koido, Hon et al. 2023). This approach can find tissue- and cell-type-specific effects of variants without any population-level dataset. Recent machine learning approaches such as convolutional neural networks enable efficient incorporation of surrounding long DNA sequences, enabling the predictions of tissue- and cell-type specific mRNA (Zhou and Troyanskaya 2015, Koido, Hon et al. 2023).

Taken together, finding active and constrained OCRs will be a promising approach to finding causal GWAS variants for complex traits and their target regulatory elements; however, lacking knowledge about constraint levels of cell-type specific OCRs hampers such application. This motivated us to infer the cell-type-specific constraint OCRs with machine learning leveraging DNA sequence patterns that may contain the evidence of constraint (Zhou, Theesfeld et al. 2018). Here, we developed a new score for OCRs, CAMBUS (Chromatin Accessibility Mutation Burden Score), to prioritize active and functional regulatory elements leveraging constraint information hidden in DNA sequences. We assessed the characteristics of CAMBUS and their cell-type specificity using OCRs in

various cell types in peripheral blood mononuclear cells (PBMCs). By leveraging CAMBUS, we cataloged 1,533 cell-type-specific putative causal variants from GWAS results for complex traits in European (EUR) and East Asian (EAS) ancestries. We demonstrated how to derive biological interpretation from GWAS findings by pinpointing the putative causal variants in a cell-type-specific manner leveraging CAMBUS.

Results

Cell-type specific OCR predictions from DNA sequences

We sorted PBMCs (peripheral blood mononuclear cells) from 54 Japanese individuals into 28 immune cell types by cell sorter and conducted ATAC-seq for the 28 cell types and PBMC (hereafter, 29 cell types) in eight subgroups (CD4; $CD4^+$ T-cells, CD8; $CD8^+$ T-cells, B; B cells, Mono; Monocytes, DC; dendritic cells, NK; Natural Killer cell, Neutrophils, and PBMC) (Figure. 1A; Supplementary Table 1). The number of cell types in this study is comparable to that in recent scATAC-seq studies using PBMC (Zhang, Wang et al. 2020, Benaglio, Newsome et al. 2023). Notably, the 29 cell types include minor cell types, such as double-negative B-cells (~5% in B-cells) (Li, Li et al. 2021). After stringent quality control, we obtained 7,939,714 OCRs that covered 498 Mb (16.1 %) of the human genome (Methods). The median number of OCRs and the size for 29 cell types were 252,668 OCRs and 276 bp, respectively. Among the 7,939,714 OCRs, 330,367 (4.2%) were observed in only one cell type, and 437,368 (5.5%) were observed in only one out of the eight subgroups. Both hierarchical clustering and dimension reduction using principal component analysis (PCA) and uniform manifold approximation and projection (UMAP) showed that these OCRs could clearly distinguish the eight subgroups but not all 29 immune cell types (Figure. S1).

Prior to calculating CAMBUS (Chromatin Accessibility Mutation Burden Score), we first examined whether machine learning (ML) models (CAMBUS ML models) can predict the OCRs of each of 29 cell types from DNA sequence patterns. For this purpose, we used the deep convolutional neural network to predict whether the OCRs overlap within the central 200bp of a 5kb input DNA sequence (Methods). We observed a notably high mean area under the receiver operating characteristic curve (AUROC) of 0.87, with a minimum of 0.84 (neutrophil), to predict OCRs across 29 cell types in the testing dataset (Figure. S2A). We observed that cell-type-specific OCRs were more challenging to predict; however, even for the OCRs observed in only one cell type, the mean AUROC was 0.73 (Figure. S2B), suggesting CAMBUS ML models could effectively capture cell-type-specific genetic architecture underlying OCRs. Notably, this level of prediction accuracy has been enough for successful downstream analyses (such as *in silico* mutagenesis for GWAS variants) in the previous studies: for example, AUROC per cell = 0.762 (Yuan and Kelley 2022) and mean AUROC for enhancer RNAs = 0.69 (Koido, Hon et al. 2023).

We also assessed the accuracy of *in silico* mutagenesis on the cell-type-specific OCRs in the 29 cell types. The direction concordance between the *in silico* mutation effects and the estimated effect size from caQTL was increased by a higher threshold of the mutation effects, as shown in previous studies (Zhou, Theesfeld et al. 2018, Koido, Hon et al. 2023). Particularly when variants were selected based on a threshold where accessibility probability changed by more than 10%, the direction concordance with caQTL effect sizes (Methods) reached 90% for the major six cell types (CD4, CD8, B, Mono, DC, and NK) (Figure. 2A; Supplementary Table 2). We also confirmed the good concordance using the independent caQTL study of lymphoblastoid cell lines (LCL; B cell lineage; Figure. 2B; Figure. S3A) (Kumasaka, Knights et al. 2016). As expected, the concordance dropped when non-B cell types were compared with the caQTL study (Figure. S3B). In total, CAMBUS ML models incorporating surrounding DNA sequence patterns could accurately

predict cell-type specific OCRs within the 29 cell types and mutation effects on these OCRs in a cell-type specific manner.

CAMBUS to find constrained OCRs

To infer constraint levels in the OCRs, we calculated *in silico* saturated mutation effects, quantifying the predicted changes in accessibility probability for all possible single nucleotide mutations within 2kb of each OCR, inspired by the previous study working on transcript expression levels (Zhou, Theesfeld et al. 2018)(Methods). We aggregated and took the mean of mutation effects within 2kb of each OCR and called this value CAMBUS. Hereafter, we defined OCRs with negative CAMBUS as CAMBUS+ (where the '+' denotes positive constraint) based on the local false discovery rate (FDR) method (Figure. 3A, 3B; Method). Besides, we defined a more relaxed CAMBUS+ set by extracting the bottom 5% of the overall CAMBUS distribution as relaxed CAMBUS+ OCRs. The median number of CAMBUS+ OCRs was 1,584, covering 0.056% of the human genome, while that of relaxed CAMBUS+ OCRs was 12,632, covering 0.33%. Notably, read counts from ATAC-seq were not a determinant factor for CAMBUS+ OCRs (Figure. S3A), reinforcing that our machine-learning approach incorporated information from DNA sequence patterns into OCRs**,** not from technical fluctuations or noises.

To confirm our key assumption that CAMBUS+ OCRs (or relaxed CAMBUS+ OCRs) are under positive constraint, we first assessed whether CAMBUS+ OCRs overlapped with evolutionarily conserved regions, as defined by phylogenetic P-values (phyloP) scores derived from conservation across 46 vertebrate species (Pollard, Hubisz et al. 2010). As expected, phyloP scores in CAMBUS+ OCRs were significantly higher than those in control OCRs across 29 cell types (Method; for example, two-sided *t*-test $P < 1.1 \times 10^{-4}$ CAMBUS+ OCRs in NaiveCD4; Supplementary Table 3). Next, we assessed whether CAMBUS+ OCRs are correlated to the genomic non-coding constraint of haploinsufficient variation

(Gnocchi), a constraint metric estimated by comparing observed allele counts in diverse human populations with the estimated counts in each 1kb region of the human genome (Chen, Francioli et al. 2024). Following the previous study (Chen, Francioli et al. 2024), we evaluated the odds ratio (OR) of CAMBUS+ OCRs for the region with Gnocchi ≥ 4, comparing with the OR of the known candidate regulatory elements: ENCODE cCREs (promoter-like, proximal enhancer-like, distal enhancer-like, and CTCF-only cCREs), FANTOM5 enhancers, and super-enhancers. The CAMBUS+ OCRs showed the strongest constraint (OR=11.45 (95% confidence interval (CI) 9.33–14.05), $P=4.7 \times 10^{-68}$ by Fisher's Exact test) among the compared regulatory elements (Figure. 3C; Supplementary Table 4). Meta-analysis demonstrated the consistent tendency across the 29 cell types (OR=8.71 (95% CI 7.85–9.66), $P=3.1 \times 10^{-365}$ from random-effect meta-analysis; Figure. 3D). Notably, the pooled OR was also greater than that of the ENCODE promoter-like regulatory elements, the strongest constraint candidate regulatory elements in the Gnocchi-proposing paper (OR=7.3) (Chen, Francioli et al. 2024), indicating that CAMBUS+ could find OCRs under very strong positive constraints. The relaxed CAMBUS+ OCRs also showed the same but weaker tendency (Figure. S3B).

Previous studies (Silvert, Quintana-Murci et al. 2019) demonstrated that enhancers, especially those activated in T-cells, are enriched in archaic genome sequences due to positive selection. Consistently, we observed that CAMBUS+ OCRs showed significant enrichment in the selection signals (Nait Saada, Kalantzis et al. 2020) (OR=1.4 (95% CI 1.3–1.5), $P=1.1 \times 10^{-26}$ from random-effect meta-analysis; Figure. S3C), the Neanderthal genome sequences observed in the Japanese population (Liu, Koyama et al. 2024) (OR=1.4 (95% CI 1.4–1.5), $P=4.8 \times 10^{-32}$ from random-effect meta-analysis; Figure. S3D), and the Neanderthal and Denisovans' sequences observed in 1000 Genomes populations (Supplementary Table 5) (Browning, Browning et al. 2018).

In addition, we observed CAMBUS+ OCRs showed significant enrichment in the pathogenic regulatory variants cataloged in the Human Gene Mutation Database (HGMD) (OR=2.70 (95% CI 2.43–2.99), P = 1.7 x 10^{-77}; from random-effect meta-analysis; Figure. S3E; Supplementary Table 6).

Enrichment of active regulatory elements by selecting CAMBUS+ OCRs

All OCRs obtained in this study were well overlapped with the known candidate regulatory elements; for example, 73.66% of all OCRs in NaiveCD4 were overlapped with super-enhancers (the median of 29 cell type is 74.70%) and 4.49% with FANTOM5 enhancers (the median of 29 cell type is 5.10%; Supplementary Table 7), both of which are known to be enriched for causal variants (Hnisz, Abraham et al. 2013). We further explored that CAMBUS+ OCRs could aid in prioritizing functional regulatory elements (Methods). For example, CAMBUS+ OCRs in NaiveCD4 significantly enriched the known regulatory elements, especially for active enhancers like super-enhancers (OR=9.07 (95% CI 6.80–12.11), Fisher's exact test P = 2.0 × 10^{-102}) and FANTOM5 enhancers (OR=6.16 (95% CI 5.39–7.03), Fisher's exact test P = 6.3 x 10^{-111}) (Supplementary Table 8). Meta-analysis showed a consistent trend across 29 cell types (OR=6.63 (95% CI 5.50–7.99), P = 1.1 x 10^{-87} from random-effect meta-analysis for super-enhancers; Figure. S3F, and OR=5.19 (95% CI 4.87–5.54), P = 4.9 x 10^{-547} from random-effect meta-analysis for FANTOM5 enhancers; Figure. S3G). Remarkably, after adjusting with known constraint metrics (Gnocchi and phyloP), we still observed statistically significant enrichment for prioritizing regulatory elements by CAMBUS+ OCRs across the 29 cell types (Figure. 3E; Supplementary Table 9). Reflecting the characteristics of the analyzed cell types (blood and immune cell types), a comparison of enrichment across four tissues (blood/hematopoietic, brain, kidney, and lung) revealed the strongest prioritization of blood's regulatory elements by NaiveCD4 CAMBUS+ OCRs (super-enhancers; OR=6.83 (95% CI 6.07–7.71), P=1.1 × 10^{-217};

FANTOM5 enhancers; OR=7.64 (95% CI 6.64–8.78), P=8.7 x 10^{-179} from logistic regression; Figure. 3F; Supplementary Table 10). This pattern was consistently observed across 29 cell types (Supplementary Table 11). We also confirmed that the relaxed CAMBUS+ OCRs exhibited the same but weaker tendency (Figure. S3H; Supplementary Table 12). Taken together, CAMBUS+ OCRs (and relaxed CAMBUS+ OCRs) effectively capture cell-type-specific active regulatory elements under positive constraints, particularly enhancers, that were not well captured by the previous method.

Heritability enrichment of CAMBUS+ in blood-relevant diseases and traits

We computed heritability enrichments in CAMBUS+ OCRs using stratified LD score regression (S-LDSC) conditioning on known functional annotations and all OCRs from this study (Methods). We used GWAS summary statistics for 33 complex traits, including 14 immune-mediated traits (e.g., multiple sclerosis (MS), rheumatoid arthritis (RA), and Atopic dermatitis (AD)), from European (EUR) and East Asian (EAS) populations (Supplementary Table 13). To avoid false positives (Tashman, Cui et al. 2021), we used the relaxed CAMBUS+ OCRs (the median proportion of single nucleotide polymorphism (SNPs) across the 29 cell types was 0.5%) for primary analyses instead of the CAMBUS+ OCRs (the median was 0.07%).

As a result, the highly significant heritability enrichment was observed in a wide variety of immune-mediated diseases (FDR < 5%; Figure. 4A; Supplementary Table 14). Particularly, plausible pairs of immune traits and cell types were observed to show the strongest enrichment of heritability among the 29 cell types: MS and T_h17 (Moser, Akgun et al. 2020), and systemic lupus erythematosus (SLE) and B cells (Jarvinen, Hellquist et al. 2012, Fillatreau, Manfroi et al. 2021) (Figure. S4A). Besides, other plausible pairs included pairs of RA with CD4 or CD8, and AD with CD4 (particularly Th2 (Honda and Kabashima 2020)), or CD8.

Based on these results, we hypothesized that polygenic risk scores (PRS) prioritized by CAMBUS+ OCRs could enhance their predictive ability. To evaluate this hypothesis, we focused on CAMBUS+ OCRs in double-negative B cells (DN B), which showed significant enrichment for the heritability of SLE in EAS ancestry (Figure. S4A) and was also known for its functional associations with SLE (Chung, Gong et al. 2023). We constructed the PRS based on variants overlapping CAMBUS+ OCRs and evaluated the additional performance to the conventional PRS using five-fold cross-validation using 137,620 individuals of EAS ancestry (1,178 cases and 136,442 controls; Methods) (Yin, Kim et al. 2021). We performed logistic regression on the five validation datasets to estimate the effect sizes of the PRS derived from the additional variants, conditioning on the conventional PRS. A fixed effect meta-analysis demonstrated that the additional variants significantly improved the predictive performance of PRS ($P = 3.12 \times 10^{-6}$; Supplementary Table 15; Methods).

Putative causal variants were enriched in CAMBUS+ OCRs

We assessed whether CAMBUS+ OCRs could prioritize the putative causal variants for complex traits, using the large-scale statistically fine-mapping studies in 94 traits in EUR ancestry (Kanai, Ulirsch et al. 2021) and 62 traits in EAS ancestry (Koyama, Liu et al. 2024). We intersected CAMBUS+ OCRs and the putative causal variants and cataloged 1,210 and 323 for trait-related cell-type-specific putative causal variants in both EUR and EAS ancestries, respectively (Methods). The CAMBUS+ OCRs were significantly enriched for all variants in 95% credible sets (median OR:3.85 and 3.94 in EUR and EAS, respectively, Figure. S5A). In line with a data source of OCRs, CAMBUS+ OCRs exhibited significantly higher enrichment for the putative causal variants of leukocyte-related traits than non-hematopoietic traits (two-sided *t*-test $P = 1.0 \times 10^{-11}$ in EUR ancestry and 1.4×10^{-2} in EAS ancestry; Figure. S5B). As an example, the enrichment of CAMBUS+ OCRs for type 1 helper T-cells was stronger among variants with high posterior inclusion probability (PIP)

(>0.9) for hematopoietic traits in EAS ancestry than those with low PIP (≤ 0.1) (OR=7.62 (95% CI 3.60−16.18), P = 1.2 x 10^{-7} from logistic regression; Figure. 5A), and this enrichment was further increased when restricted in the leukocyte traits (OR=11.0 (95% CI 4.04–29.96), P = 2.7 x 10^{-6}; Figure. 5A). Meta-analysis showed this trend was consistent across 29 cell types (OR=8.99 (95% CI 7.85–10.29), P = 8.8 x 10^{-221} for EUR ancestry; OR=19.24 (95% CI 16.03 – 23.09), P = 3.9 x 10^{-221} for EAS ancestry; Figure. 5B). The median regional length of CAMBUS+ (845 bp) was much shorter than that of 95% credible sets (3.0M bp for EUR ancestry and 1.1M bp for EAS ancestry). Taken together, CAMBUS+ OCRs can pinpoint or at least narrow down causal variants. Notably, even for rare variants (minor allele frequency (MAF) < 0.01), the putative causal variants of hematopoietic traits were significantly enriched in CAMBUS+ OCRs in at least one cell type (Methods; OR=4.68 (95% CI 2.66–7.99), two-sided Fisher's exact test P = 2.23 x 10^{-6}; Figure. 5C). This suggested that CAMBUS+ OCRs can potentially prioritize even rare causal variants from GWAS results which are difficult to prioritize in the conventional statistical fine-mapping (Schaid, Chen et al. 2018).

Leveraging the overlapped putative causal variants, we found plausible examples of putative causal variants where CAMBUS+ OCRs led to the biological interpretation of GWAS findings. First, we found that rs8009224 was the only one that overlapped with CAMBUS+ OCRs of plasmablast (Figure. S6A) among the seven putative causal variants for hemoglobin A1c levels. This is an intronic variant of *MIDEAS* (Mitotic Deacetylase Associated SANT Domain Protein), which is low frequent in both 1KG EUR (MAF = 3.4%) and EAS (MAF = 1.2%) and also associated with mean corpuscular hemoglobin concentration (Barton, Sherman et al. 2021). The overlapping regulatory element was connected to the 16 genes by the Activity-by-Contact (ABC) model's prediction (ABC enhancer) in B-cell, and the putative target gene with the second highest ABC score is

MIDEAS (ABC score = 0.097, much higher than the proposed threshold corresponding to 70% recall and 59% precision)(Fulco, Nasser et al. 2019). Second, rs13122305 was the only one overlapping with CAMBUS+ OCRs in monocytes among seven candidate causal variants in a credible set for monocyte count (Figure. 6A). The nearest gene of this variant is *COQ2*, whose anti-inflammatory functions via regulating gene expression were reported (Armanfar, Jafari et al. 2015, Mantle, Heaton et al. 2021). Additionally, we found that the ABC enhancer in monocytes only overlapped with rs13122305 and that *COQ2* was also supported by the ABC model with the second-highest ABC score (0.025) among the eight target genes. Third, among the three candidate causal variants in a credible set in the FCGR region for Albumin/Globulin ratio (AG), only rs2487451 overlapped with non-classical Monocyte CAMBUS+ OCR. Non-classical monocyte, known to display antigen presenting properties (Mukherjee, Kanti Barman et al. 2015), were the only cell type among 29 cell types whose OCR overlapped with a candidate causal variant. The nearest gene was *FCGR3B*, encoding a receptor (FcγRIIIB) that binds to the Fc region of IgG (Immunoglobulin) antibodies, which is known to be expressed in non-classical monocytes (Nassir, Tambi et al. 2021). Fourth, rs55646091, a putative causal variant for asthma (PIP = 0.99), overlapped with CAMBUS+ OCR of regulatory T-cells (Figure. 6B) among the 29 cell types. The nearest gene of this variant was *LRRC32* (leucine-rich repeat-containing 32) which was potentially involved in Asthma (Li, Wang et al. 2023) and whose encoding protein was known as a surface marker for T-reg. Furthermore, this variant-gene pair was also supported by the ABC model and *LRRC32* displayed the highest ABC score (ABC score = 0.041 that is much higher than the threshold corresponding to 70% recall and 59% precision)(Fulco, Nasser et al. 2019) among the nine genes connected with the regulatory element overlapping with the OCR and the variant. Lastly, we demonstrated that CAMBUS+ in regulatory T-cells could prioritize only one putative causal variant

(rs9814991) from too many variants (fifty-seven) in this credible set for eosinophils count (Figure. S7B).

Discussion

This study proposed CAMBUS+ OCRs that can mark active and functional regulatory elements from all OCRs by only leveraging constraint information in surrounding DNA sequence patterns using the reference genome. These OCRs exhibited strong enrichment in regulatory elements, particularly tissue-specific active enhancers, even after being adjusted for known constraint metrics (Gnocchi and phyloP). Furthermore, heritability for many complex traits was strongly enriched in CAMBUS+ OCRs regions. CAMBUS+ OCRs effectively prioritized putative causal variants for immune-related traits, even rare causal variants. Thus, CAMBUS+ OCRs will provide biological insights from GWAS, especially immune-related traits.

We developed CAMBUS focusing on constraints by assuming that DNA sequencing patterns surrounding OCRs contain hidden information related to their constraints. An alternative potential approach using ATAC-seq (or DNase-seq) could prioritize regions with high accessibility (i.e., regions with many read counts). However, previous studies have suggested no relationship between accessibility and functionality or constraints (Roadmap Epigenomics, Kundaje et al. 2015, Kuderna, Ulirsch et al. 2024, Martens, Fischer et al. 2024). Consistently, accessibility was not a determinant factor in defining CAMBUS+ OCRs. Thus, leveraging surrounding DNA sequence patterns through machine learning offers a unique and effective strategy for identifying biologically important OCRs.

We demonstrate that CAMBUS+ OCRs can effectively prioritize causal rare variants for complex traits. A previous study showed that rare variants tend to be enriched

in the constraint genome (Karczewski, Francioli et al. 2020), consistent with our study as CAMBUS+ OCRs can mark such constrained regions. In GWAS using SNP arrays, low statistical power and low imputation accuracy for rare variants make it difficult to detect rare variant associations and identify causal rare variants through statistical fine-mapping. Despite these challenges, CAMBUS+ OCRs can facilitate the rare variant prioritization that might otherwise be missed.

Eosinophilic asthma is a subtype characterized by elevated levels of eosinophils (Nelson, Bush et al. 2020). In this analysis, we identified a variant (rs55646091) associated with asthma linked to increased eosinophil counts (PIP = 0.03). Both traits exhibit positive effect sizes (0.20 for asthma, 0.072 for eosinophil counts), suggesting that carriers of this variant experience elevated eosinophil levels, which contribute to inflammation and the onset of asthma (Harb and Chatila 2023). Notably, this variant overlaps specifically with T-regulatory (T-reg) cells among 29 blood cell types analyzed. The nearest gene of this variant is LRRC32, a known surface marker of T-reg cells, which has been previously implicated in immune regulation (Tran, Andersson et al. 2009). The findings from this analysis provide additional evidence supporting a biological mechanism in which the variant, through its effects on T-reg cells, leads to increased eosinophil counts, thereby contributing to the development of asthma. This insight deepens our understanding of the role of T-reg cells and LRRC32 in asthma pathogenesis, particularly in eosinophilic inflammation.

In this study, we focused on various immune cell types; however, our approach is not restricted to immune cell types and can be applicable to other organs and tissues, such as neural cells and skin cells. As GWAS results continue to accumulate, integrating CAMBUS+ OCRs with these expanding GWAS results has the potential to uncover further insights into the regulatory mechanisms underlying complex traits. This method can be applicable to OCRs identified from single cells. Taken together, CAMBUS+ OCRs not only capture constrained and functional regulatory elements but also facilitate the interpretation

of non-coding GWAS variants for complex traits by prioritizing causal variants in a cell-type-specific manner without relying on LD information.

Method

Sample and library preparation

We collected peripheral blood (PB) cells from 54 healthy Japanese volunteers and sorted them into 29 cell types. PBMCs were isolated by density gradient separation with Ficoll-Paque (GE healthcare) immediately after blood drawing. Erythrocytes were lysed with potassium ammonium chloride buffer, and non-specific binding was blocked with Fc-gamma receptor antibodies. PBMC stained with cell surface specific antibodies (Supplementary Table 22). 27 immune cell populations were sorted by FACS (BDAria III) using the gating strategy (Supplementary Table 1). In addition, neutrophils were isolated by MACSxpress Neutrophil Isolation Kits human (Miltenyi Biotec) from 4 × 106 PBMC cells. Sorted cells, isolated PBMC, and Neutrophils were stored at −80°C in CytoStor-10 (Charles River Laboratories Cell Solutions). Libraries for ATAC-seq were prepared using a modified protocol of Omni-ATAC (Corces, Trevino et al. 2017). Genomic DNA from whole blood was isolated using QIAamp DNA Blood Mini Kits, respectively. ATAC-seq was performed using 150bp paired-end on Illumina NovaSeq6000. In total, we obtained a median of 13.34M (+/-7.56M) reads per sample. This study was approved by the Ethics Committees of RIKEN. Written informed consent was obtained from each volunteer.

Mapping ATAC-seq data

ATAC-seq data were processed following the ENCODE ATAC-seq pipeline (version 1.8.0) as follows: Raw reads were trimmed using cutadapt (version 2.5) and aligned to human genome assembly GRCh38 analysis set using bowtie2 (version 2.3.4.3) for each sample.

After alignment, duplicated reads were removed using MarkDuplicates (Picard version 2.20.7-SNAPSHOT), retaining uniquely mapped reads and improperly paired reads using samtools (version 1.9), and removed reads that mapped to the mitochondrial genome.

In total, we obtained a median of 5.39M (s.d. 3.28M) QCed reads per sample.

ATAC-seq peak calling

For each 29 immune cell type, we used the samtools merge command to merge the QCed reads for each cell type, and used MACS2 (version 2.1.1) to identify the ATAC-seq peaks (OCRs) following a recent study (Gate, Cheng et al. 2018) with parameters (-p 0.01 --shift -75 –extsize 150 --nomodel). We obtained a median of 253,553 ($\pm$66,738) OCRs with a median peak width of 271bp ($\pm$18bp) (FDR<0.05). Using the alignment file for each cell type, we calculated the read counts for each OCR with bedtools (version 2.30.0)'s coverage function.

Quality control for ATAC-seq dataset

We first assessed the quality of ATAC-seq data using Pearson correlations of chromatin accessibility among the samples for each cell type, using 614,516 peaks that were identified from across all samples using the same parameters described above (these peaks were only used for the quality control purpose). We filtered OCRs out when the Pearson correlations were not greater than 0.65 (determined by manual inspection of the distribution of these correlations). Additionally, we excluded outlier samples with low Pearson correlations by visual inspection (Supplementary Table 16). Samples with a mapped rate of less than 0.5 were further excluded. Finally, we obtained 1,386 samples (the median number of donors per cell type is 48; Supplementary Table 1).

Hierarchical clustering and dimension reduction

We first chose the top 5,000 accessible OCRs (defined by TPM) from each cell type and merged them across 29 cell types, resulting in a total of 145,000 unique regions. We then created a binary matrix (0, 1) to indicate whether each 300bp bin across the genome was overlapped by the corresponding OCRs. Hierarchical clustering was performed using Ward's method of Euclidean distance using the binary matrix. PCA for the binary matrix was performed using the binaryPCA function from the scBFA package (version 1.16.0) (Li and Quon 2019) in R with default parameter. UMAP was performed with the top five PCs using the umap function from the scikit-learn package (version 0.18.1) in Python with default parameters.

Strategy for the CAMBUS ML model

The CAMBUS ML model was built upon the DeepSEA architecture, a deep CNN model (Zhou and Troyanskaya 2015). We used the Selene library (v0.4.7) to train the CAMBUS ML model. A 5kb reference sequence, randomly chosen with Selene, is used as input features, five times longer than the sequence used in the original DeepSEA model to capture broader genomic contexts. The model outputs a sigmoid function-derived score, which can be interpreted as a proxy for the likelihood that the OCRs overlap with the central 200bp of the input sequence (see Supplementary Table 17 for the configuration details). We referred to this predicted probability for chromatin accessibility as the accessibility probability.

We combined 7,939,714 OCRs across 29 cell types using the `bedtools merge` function and obtained 1,349,934 non-overlapping unique input sequences. According to Selene's default settings, we used chromosomes 8 and 9 as testing, chromosomes 6 and 7 as

validation, and the other autosomal chromosomes as training data. The details of Selene's parameters are described in Supplementary Table 17.

In silico saturated mutagenesis using the trained CAMBUS ML model

For all bases within 1kb from the center of each OCR, we used the trained CAMBUS ML model to calculate the predictions for all possible single-based mutations. This comprehensive approach provides an unbiased analysis of mutational effects across the entire sequence, rather than focusing on only specific known polymorphisms. To quantify the mutation effect, we calculated the difference in log fold changes of predictions between the reference and alternative alleles for each site and averaged them across all bases. In total, we obtained 505 million mutation effects (median across the 29 cell types).

Validation of CAMBUS ML model with *in silico* mutagenesis

We compared the *in silico* mutation effects predicted by the CAMBUS ML model with effect sizes from the caQTL study. The samples for caQTL (n=74, including additional independent samples to increase statistical power) were genotyped using Infinium ASA-24+v1.0 kit, and whole genome imputation was conducted after stringent quality control (Supplementary Table 18). The caQTLs were mapped using RASQUAL (v1.1) with default parameters. The permutation to empirically obtain the null distribution for each region was performed with default parameters, resulting in a median of 654 lead caQTLs with FDR < 0.1, which we compared against the *in silico* mutation effects. Additionally, we calculated the *in silico* mutation effects for 297,308 autosomal lead SNVs in the previous study's caQTL. The positions of those lead SNVs were mapped to the hg38/GRCh38 coordinate using the liftOver tool with the hg19ToHg38.over.chain file to be consistent with our study. To further refine the comparison, we filtered the target caQTL peaks>50% overlapping with

our OCRs and selected the variants inside the peak. In total, we used 156,039 caQTLs peak pairs to compare with the mutation effect.

Identification of putative constraint open chromatin region

We modeled the distribution of the mean mutation effect (*in silico* saturated mutagenesis) within 2kb of each OCR (CAMBUS) as a mixture of a Gaussian null distribution. We hypothesized that the OCRs with negative CAMBUS are likely positive constraint regions and OCRs with neither negative nor positive CAMBUS as control OCRs. We calculated local FDR with the locfdr function in the locfdr R package (version 1.1-8) for each cell type. This analysis identified a median of 1,584 putative positive constraint OCRs across 29 cell types with FDR < 0.5, referred to as CAMBUS+ OCRs, and a median of 248,749 control OCRs across 29 cell types (Zhou, Theesfeld et al. 2018). We also defined relaxed CAMBUS+ OCRs by extracting the bottom 5% of the CAMBUS distribution for each cell type (Supplementary Table 19).

Enrichment of CAMBUS+ OCRs in constraint regions

We evaluated whether CAMBUS+ OCRs are enriched in constraint regions of the genome using Gnocchi. We used the 1,984,900 QCed Gnocchi (see URLs) and calculated the OR following the methodology described in the previous paper (Chen, Francioli et al. 2024) for 1,843,559 non-coding 1-kb windows. In brief, we counted the number of overlapping 1kb windows within the following bins: (∞, -4), [−4,−3), [−3,−2), [−2,−1), [−1,−0), [0,1), [1,2), [2,3), [3,4), [4,∞) with each CAMBUS+ OCR. ORs were calculated by comparing these overlaps with all 1kb windows. Fisher's exact test was conducted to estimate the statistical

significance (p-value). The OR of the known regulatory elements for each bin was obtained from the gnomAD download site (see URLs) and used for the comparison.

To calculate the enrichment of the phyloP score in CAMBUS+ OCRs, we used the scores for all 46 species (see URLs) and mapped the positions of those datasets to the hg38/GRCh38 coordinate using liftOver as described previously. The overlapping regions were considered to be overlapped if they had more than 50% overlap with each other.

Correlation between CAMBUS and regulatory elements

We evaluated the functional enrichment of CAMBUS+ OCRs in known regulatory elements, including ENCODE cCREs, FANTOM5 enhancers, and super-enhancers (see URLs). For each CAMBUS+ OCR, we counted overlapping annotations for each known regulatory element and, calculated the OR compared with all OCRs, and tested it using Fisher's exact test, as described in the previous section. For tissue-expressed FANTOM5 enhancers, we obtained count per million (CPM) data for 249,599 enhancers across 347 tissue/cell types with hg19 coordinates (see URLs) and selected enhancers expressed in hematopoietic_cell (N = 163), brain (N = 85), kidney (N = 16), and lung (N = 8) based on a threshold of CPM >= 0.1 in at least 10% of individuals in each enhancer. As described previously, the positions were mapped to the hg38/GRCh38 coordinate using liftOver. For tissue-expressed super-enhancers, we obtained Blood (N = 115), brain (N = 203), kidney (N = 34), and lung (N = 119) enhancers with hg38 coordinates (see URLs) and merged these enhancers by tissue with `bedtools merge` function. The adjusted OR with Gnocchi and phyloP was estimated using a logistic regression model, adjusting for the average Gnocchi and pyhoP of overlapping CAMBUS+ OCRs and control CAMBUS OCRs.

For all analyses, regions were considered to be overlapped if they had more than 50% overlap with each other.

Heritability enrichment analysis

To estimate heritability enrichment in each OCR, we conducted stratified-linkage disequilibrium score regression (S-LDSC) with LDSC (ver.1.0.1) using the baseline model (version 1.2; 53 categories). The p-value of the coefficient for CAMBUS+ OCR (or relaxed CAMBUS+ OCR) was obtained by adjusting for the 53 categories in the baseline model and all OCRs in each cell type. Multiple testing correction across all trait-cell type pairs was performed to estimate FDR using the Storey method (Storey 2002). The summary statistics were obtained from Alkes Price Lab (See URLs and our previous study (Oguchi, Suzuki et al. 2024)), and five GWAS results in EAS ancestry: systemic lupus erythematosus (Yin, Kim et al. 2021), rheumatoid arthritis (Ishigaki, Sakaue et al. 2022), Systemic sclerosis (Ishikawa, Tanaka et al. 2024), Atopic dermatitis (Tanaka, Koido et al. 2021), and Takayasu arteritis (Terao, Yoshifuji et al. 2018). For this analysis, CAMBUS OCRs' positions were mapped to the hg19 coordinate using the UCSC liftOver tool with hg38ToHg19.over.chain file to be consistent with summary statistics. After mapping to hg19, regions mapped to different chromosomes were excluded from the analysis.

PRS analysis

The PRS was constructed using PLINK v1.9, following a systematic approach with p-value thresholds using SLE GWAS in EAS ancestry. To select relevant variants for the PRS, we selected SNPs that met 20 types of p-value thresholds: 1, 0.9, 0.8, 0.7, 0.6, 0.5, 0.4, 0.3, 0.2, 0.1, 0.05, 0.01, 0.005, 5.0×10^{-4}, 5.0×10^{-5}, 1.0×10^{-5}, 5.0×10^{-6}, 1.0×10^{-7}, 5.0×10^{-7} and 5.0×10^{-8}. After selecting SNPs based on these thresholds, we applied LD clumping to remove SNPs in high linkage disequilibrium (LD) using nine types of r^2 thresholds (0.1, 0.2, 0.3, 0.4, 0.5, 0.6, 0.7, 0.8, 0.9) and a 250kb physical distance. This process yielded 180 PRS models. To determine the optimal PRS model, we applied a 5-

fold cross-validation strategy. The dataset was divided into five folds, with four folds used for training and one for testing in each iteration. We computed PRSs for all 180 models using variants from SLE GWAS in EAS ancestry (Yin, Kim et al. 2021) for each training set. We calculated the AUC with pROC (v1.18.4) to select the combination of p-value and r^2 parameters that yielded the best AUC for each training set. We then took the two variant sets; (a) variants filtered with the best parameters, and (b) all variants overlapping with DN B CAMBUS+ OCRs as prioritized variants. To mitigate overfitting due to LD structures, we removed the variants with LD>0.7 with variants in set (b). We then calculated the PRS for both sets (a) and (b) for each of the five test sets, we estimated the effect size of PRS from set (b), controlling for the PRS from set (a) using a logistic regression model. Finally, we performed a fixed-effects meta-analysis to evaluate the improvement in predictive power with the prioritized variants.

Fine-mapping enrichment analysis

We downloaded the UKB fine-mapped variants of 94 complex diseases and traits from the Finucane lab (see URLs) and obtained BBJ fine-mapped variants of 62 quantitative traits from a recent study (Koyama, Liu et al. 2024). Regarding the UKB fine-mapped variants, we used PIP from the SuSiE. The positions of those datasets were mapped to the hg38/GRCh38 coordinate using liftOver as described previously. In total, we obtained 830,654 trait-variant pairs for UKB and 544,745 trait-variant pairs for BBJ. The number of overlapped variants for each trait in 29 cell types of CAMBUS+ OCRs was counted, and the OR was estimated using all OCRs in each 29-cell type as the background and calculated P-value from the logistic regression model. After Bonferroni correction (P=0.05 divided by the number of tested phenotypes), the median of OR is calculated from the significant enrichment in UKB and BBJ (Figure. S6A, B; Supplementary Table 20).

We categorized each trait into hematopoietic and non-hematopoietic. Furthermore, hematopoietic traits are categorized into leukocyte and non-leukocyte traits (Supplementary Table 21). The number of traits and variants in each category are described in Supplementary Table 21.

Then, we counted the overlap of variants for each leukocyte and non-leukocyte and non-hematopoietic for each 29 cell-type CAMBUS+ OCRs. We calculated the OR using the method described above.

To perform enrichment analysis of rare variants, we first created merged OCRs by combining CAMBUS+ OCRs from 29 different cell types (merged CAMBUS+ OCRs). The number of overlapped variants with MAF < 0.01 and PIP > 0.1 in merged CAMBUS+ OCRs was counted for all traits and only hematopoietic traits, and the OR was calculated using the variants with MAF < 0.01 and PIP <= 0.1 as the background and calculated one-sided Fisher's exact P-value.

Catalog cell-type-specific putative causal variants

We chose variants as putative causal variants from each of the credible sets overlapping only one variant with CAMBUS+ OCRs. Then, we filtered the variants that overlapped with only one cell type of CAMBUS+ OCRs. In total, we obtained 186 and 62 cell-type-specific putative causal variants. Furthermore, we chose the variants that overlapped only one subgroup (One of the CD4, CD8, B, Mono, DC, NK, Neutrophil; Supplementary Table 1). Finally, we obtained 1,210 and 323 for trait-related cell-type-specific putative causal variants from both EUR and EAS ancestries, respectively.

Statistical analysis

For p-value calculation with R, in case of insufficient precision with standard floating-point arithmetic, the Rmpfr package (ver 0.9.2) was used to handle high-precision floating-point arithmetic to calculate p-value with z-score. For the meta-analysis, the pooled OR was calculated using a random effect model with metafor R package.

URLs

Gnocchi is at https://gnomad.broadinstitute.org/downloads#v3-genomic-constraint. Enrichment for Gnocchi with the known cCREs is at gs://gnomad-nc-constraint-v31-paper/fig_tables/constraint_z_genome_1kb.annot.txt. ENCODE cCREs V3 is at https://screen.encodeproject.org/. FANTOM5 enhancer is at https://zenodo.org/record/556775/. Super enhancer is at https://bio.liclab.net/sedb/download.php. Phylop is at https://hgdownload.cse.ucsc.edu/goldenPath/hg19/phyloP46way/primates. GWAS summary statistics are at https://alkesgroup.broadinstitute.org/sumstats_formatted, and https://alkesgroup.broadinstitute.org/UKBB/. ABC predictions are at https://mitra.stanford.edu/engreitz/oak/public/Nasser2021/AllPredictions.AvgHiC.ABC0.015.minus150.ForABCPaperV3.txt.gz. UKB fine-mapped variants are at https://www.finucanelab.org/data. FANTOM5 tissue-expressed data is at https://zenodo.org/records/5348471.

Acknowledgment

We would like to thank all the participants in the study. We deeply thank all the members of the Laboratory for Statistical and Translational Genetics, RIKEN Center for Integrative Medical Sciences for the technical support. We acknowledge the use of Biorender for

aspects of the figures. This work was supported by Japan Agency for Medical Research and Development (AMED) grants 21ek0109555, 21tm0424220, 21ck0106642, 23ek0410114, and 23tm0424225. Japan Society for the Promotion of Science (JSPS) KAKENHI grant JP20H00462 and JP23K14164.

Author contributions

K.T., M.K., and C.T. conceived the study design. A.S. performed ATAC-sequencing and DNA genotyping. K.T. and N.T. performed whole genome imputation. K.T. analyzed this study with the help of S.Y., N.T., Y.I., X.L., S.K., and M.K. M.K. and C.T. supervised this study. S.Y., N.T., S.K., K.I., Y.M., Immune transcript/enhancer consortium, and K.Y. provided helpful comments and discussion. K.T., M.K., A.S., and C.T. wrote the manuscript.

Figure legends

Figure. 1 | Study design

Overview of the study design. **A**, Dataset comprising 29 cell types used to validate our approach. **B**, Machine learning model developed to predict OCRs. **C**, Identification of putative constraint OCRs (CAMBUS+). **D**, Characterization of CAMBUS+ OCRs and prioritization for putative causal variants.

Figure. 2 | Accuracy of mutation effect of CAMBUS ML model

A. Direction concordance between *in silico* mutation effect from CAMBUS ML and effect size from our caQTL study. **B**. Direction concordance between *in silico* mutation effect from

the CAMBUS ML for Naïve B and effect size from independent LCL caQTL study. The Pearson correlation coefficient (Pearson corr.) was calculated to assess the relationship between *in silico* mutation effects and eQTL effect sizes.

Figure. 3 | CAMBUS+ OCRs can mark constraint regions and active enhancers

A, Distribution of CAMBUS. The red part represents putative constraint OCRs. **B,** Genome browser view at representative constraint region around CAMBUS+ in monocytes (chr3:141,217,899-141,218,844). The black box represents Gnocchi with Z > 4, and the grey box represents Gnocchi with Z < 4. **C, D.** Enrichment (odds ratio; OR) of CAMBUS+ in non-coding Gnocchi (n = 1,843,599), comparing with the known regulatory elements (using previous study's results, see URLs) in non-coding Gnocchi (n = 1,843,599). We calculated the OR of CAMBUS+ (n = 1,266) and CAMBUS control (n = 251,807) for NaiveCD4 using various Gnocchi' thresholds in (**C**) and OR for each CAMBUS+ OCR in 29 cell types and their pooled OR through random effects meta-analysis using Gnocchi > 4 in (**D**). The blue dashed line represents the OR of ENCODE cCRE-PLS (**D**). **E**, Enrichment of CAMBUS+ OCRs for NaiveCD4 (n = 1,266) in the known cCREs (ENCODE cCRE-PLS; n = 40,891, ENCODE cCRE-pELS; n = 172,027, ENCODE cCRE-dELS; n = 789,200, ENCODE CTCF-only; n = 35,839, FANTOM5 enhancers; n = 63,280, Super enhancers; n = 16,472), adjusted for Gnocchi and phyloP. **F**, Enrichment of CAMBUS+ for NaiveCD4 (n = 1,266) in the tissue expressed FANTOM5 enhancers (hematopoietic cells; n = 64,225, Brain; n = 62,978, Kidney; n = 35,177, Lung; n = 26,630), and Super enhancers (Blood; n = 8,055, Brain; n = 9,372, Kidney; n = 4,712, Lung; n = 9,878). The dashed line represents no enrichment (OR=1.0; **C, E, F**). CAMBUS control in NaiveCD4 (n = 251,807) is used as background in (**E, F**). The error bars represent 95% confidence intervals, with only lower bounds shown in C (See Supplementary Table 4 for higher bounds).

Figure. 4 | Heritability enrichment for immune-mediated diseases

A, The heritability enrichment of various GWAS traits (in total, 33 GWAS for EUR and EAS ancestries; Supplementary Table 13) in CAMBUS+ OCRs for each of 29 cell types. The heatmap colors indicate -log10-scale p-value of the coefficient for CAMBUS+ annotation in S-LDSC (coefficient P). '*' indicates significance (qvalue < 0.05) after FDR correction.

Figure. 5 | Enrichment analysis for putative causal variants in CAMBUS+ OCRs

A, Enrichment of putative causal variants in leukocyte (leuko), non-leukocytes (non_leuko), hemato (leuko + non_leuko), and non-hematopoietic (non_hemato) traits in CAMBUS+ OCRs for Th1. Putative causal variants were obtained from statistical fine-mapping analysis of many complex traits' GWAS results for EAS and EUR populations (Kanai, Ulirsch et al. 2021, Koyama, Liu et al. 2024). **B**, Forest plot showing the enrichment of CAMBUS+ OCRs across 29 cell types and the pooled OR in highly confident putative causal variants (PIP > 0.9). Variants with PIP <= 0.1 were used as the background for OR calculation. **C,** Enrichment of CAMBUS+ OCRs for any of 29 cell types in putative causal rare variants (maf < 0.01 in EAS), evaluated by comparing the proportion of CAMBUS+ OCRs overlapping with putative causal rare variants with PIP > 0.1. The left dot represents the OR calculated using all the putative causal variants, while the right dot represents the OR based only on the putative causal variants for hematopoietic phenotypes. The dashed line represents no enrichment (OR=1.0).

Figure. 6 | Prioritization of putative causal variants using CAMBUS+ OCRs

A, B, Representative examples of variants associated with monocyte counts prioritized with CAMBUS+ in Mono (**A**) and asthma prioritized with CAMBUS+ in regulatory T-cells (**B**) in putative causal variants in EUR ancestry and surrounding genomic annotations. The navy

boxes represent putative causal variants in this credible set. The blue dashed line represents an enhancer-gene connection to the nearest protein-coding gene predicted by the ABC model for $CD14^+$ monocytes (**A**) and HUVEC (**B**). The gene with the highest ABC score is also shown in (**A**). All the other CAMBUS+ OCRs around putative causal variants (rs13122305 (**A**), rs55646091 (**B**)) are also shown in the figures (The purple box represents PBMC).

Supplementary Figure

Figure. S1 | Clustering analysis and dimension reduction using PCA and UMAP

(**A**) Hierarchical clustering, (**B**) PCA, and (**C**) UMAP (**C**) of 1,386 samples. The top 5,000 most accessible OCRs were used for these analyses. The colors indicate the classification of samples into eight subgroups across 29 cell types. **D**, UMAP of 1,386 samples (**C**) colored by eleven types of CD4; other subgroups are colored with grey.

Figure. S2 | Accuracy of CAMBUS ML models

A, Predictive accuracy of the CAMBUS ML models across 29 cell types. The dashed line represents the mean AUROC across the 29 cell types (0.87). **B,** Specificity of CAMBUS ML models with respect to OCR sharing. The x-axis shows the number of cell types sharing OCRs. For example, the leftmost category represents OCRs shared among 20 to 28 cell types, and the rightmost category indicates OCRs unique to a single cell type.

Figure. S3 | Accuracy of *in silico* mutation effect

A, Comparison of direction concordance between *in silico* mutation effects predicted by the CAMBUS ML models (across five B-cell types) and effect sizes from an independent LCL

caQTL study. The Pearson correlation coefficient (Pearson corr.) was calculated to assess the relationship between *in silico* mutation effects and eQTL effect sizes. The x-axis represents a threshold of *in silico* mutation effects to calculate direction concordance, where 'all' indicates no threshold was applied. **B,** Comparison of direction concordance between *in silico* mutation effects from the CAMBUS ML models and effect size from the LCL caQTL study. Absolute *in silico* mutation effects greater than > 0.1 are used (see Figure. 2A).

Figure. S4 | CAMBUS+ can mark constraint regions and active enhancers

A, Scatter plot of median TPM and CAMBUS in Naïve CD4. The vertical dashed line represents the top 5% of the median TPM. **B,** OR of relaxed CAMBUS+ OCRs across 29 cell types in Gnocchi> 4 and pooled OR estimated through random effect meta-analysis. The blue dashed line represents the OR of ENCODE promoter-like elements. **C, D, E, F, G,** OR and the pooled OR of the CAMBUS+ OCRs in UKB selection signals (**C**), Neanderthal genome sequences derived from samples of EAS ancestry (**D**), pathogenic regulatory variants (**E**), super-enhancers (**F**) and FANTOM5 enhancers (**G**). **H,** ORs of relaxed CAMBUS+ (NaiveCD4; n = 12,736) in cell-type specific regulatory elements: the tissue expressed FANTOM5 enhancers (hematopoietic cells; n = 64,225, Brain; n = 62,978, Kidney; n = 35,177, Lung; n = 26,630), and super-enhancers (Blood; n = 8,055, Brain; n = 9,372, Kidney; n = 4,712, Lung; n = 9,878). The dashed line represents no enrichment (OR=1.0; **B**, **C, D, E, F, G, H**)

Figure. S5 | Heritability enrichment for immune-mediated diseases

A, The -log10-scale coefficient P of CAMBUS+ OCRs in 29 cell types for SLE GWAS in EAS ancestry. The dashed line indicates coefficient P = 0.05. '*' indicates significance (qvalue < 0.05) after FDR correction.

Figure. S6 | Prioritization of putative causal variants using CAMBUS+ OCRs

A, Median OR of all variants in 95% credible sets in CAMBUS+ OCRs across 29 cell types. We used putative causal variants from statistical fine-mapping studies in EUR and EAS ancestries (Kanai, Ulirsch et al. 2021, Koyama, Liu et al. 2024). The solid line represents the median OR across 29 cell types. **B**, Enrichment of the putative causal variants in leukocyte (leuko), non-leukocytes (non_leuko), and non-hematopoietic (non_hemato) traits in CAMBUS+ OCRs across 29 cell types. Only cell types with P < 0.05 are shown (27 cell types in BBJ leuko; 28 in UKB non_hemato; 29 in BBJ non_leuko, BBJ non_hemato, UKB leuko, and UKB non_leuko), and dot indicate -log10-scale p-value. t-tests were performed between leuko and non_hemato traits, with significance levels denoted as P <0.05 ('*') and P < 0.001 ('***').

Figure. S7 | Prioritization of putative causal variants using CAMBUS+ OCRs

A, **B** representative example of variants associated with Hemoglobin A1c level prioritized with CAMBUS+ in plasma blast in putative causal variants in EUR ancestry (**A**) and eosinophils prioritized with CAMBUS+ in regulatory T-cell (**B**) and their surrounding genomic annotations. The navy boxes represent putative causal variants in the credible set. The blue dashed line represents an enhancer-gene connection to the nearest protein-coding gene predicted by the ABC model in B-cells (**A**). All the other CAMBUS+ OCRs around putative causal variants (rs8009224 (**A**)) are also shown in the figures (The purple box represents PBMC).

References

Andersson, R., C. Gebhard, I. Miguel-Escalada, I. Hoof, J. Bornholdt, M. Boyd, Y. Chen, X. Zhao, C. Schmidl, T. Suzuki, E. Ntini, E. Arner, E. Valen, K. Li, L. Schwarzfischer, D. Glatz, J. Raithel, B. Lilje, N. Rapin, F. O. Bagger, M. Jorgensen, P. R. Andersen, N. Bertin, O. Rackham, A. M. Burroughs, J. K. Baillie, Y. Ishizu, Y. Shimizu, E. Furuhata, S. Maeda, Y. Negishi, C. J. Mungall, T. F. Meehan, T. Lassmann, M. Itoh, H. Kawaji, N. Kondo, J. Kawai, A. Lennartsson, C. O. Daub, P. Heutink, D. A. Hume, T. H. Jensen, H. Suzuki, Y. Hayashizaki, F. Muller, A. R. R. Forrest, P. Carninci, M. Rehli and A. Sandelin (2014). "An atlas of active enhancers across human cell types and tissues." Nature **507**(7493): 455-461.

Andrews, G., K. Fan, H. E. Pratt, N. Phalke, s. Zoonomia Consortium section, E. K. Karlsson, K. Lindblad-Toh, S. Gazal, J. E. Moore and Z. Weng (2023). "Mammalian evolution of human cis-regulatory elements and transcription factor binding sites." Science **380**(6643): eabn7930.

Armanfar, M., A. Jafari, G. R. Dehghan and L. Abdizadeh (2015). "Effect of coenzyme Q10 supplementation on exercise-induced response of inflammatory indicators and blood lactate in male runners." Med J Islam Repub Iran **29**: 202.

Barton, A. R., M. A. Sherman, R. E. Mukamel and P. R. Loh (2021). "Whole-exome imputation within UK Biobank powers rare coding variant association and fine-mapping analyses." Nat Genet **53**(8): 1260-1269.

Benaglio, P., J. Newsome, J. Y. Han, J. Chiou, A. Aylward, S. Corban, M. Miller, M. L. Okino, J. Kaur, S. Preissl, D. U. Gorkin and K. J. Gaulton (2023). "Mapping genetic effects on cell type-specific chromatin accessibility and annotating complex immune trait variants using single nucleus ATAC-seq in peripheral blood." PLoS Genet **19**(6): e1010759.

Browning, S. R., B. L. Browning, Y. Zhou, S. Tucci and J. M. Akey (2018). "Analysis of Human Sequence Data Reveals Two Pulses of Archaic Denisovan Admixture." Cell **173**(1): 53-61 e59.

Buenrostro, J. D., P. G. Giresi, L. C. Zaba, H. Y. Chang and W. J. Greenleaf (2013). "Transposition of native chromatin for fast and sensitive epigenomic profiling of open chromatin, DNA-binding proteins and nucleosome position." Nat Methods **10**(12): 1213-1218.

Chen, S., L. C. Francioli, J. K. Goodrich, R. L. Collins, M. Kanai, Q. Wang, J. Alfoldi, N. A. Watts, C. Vittal, L. D. Gauthier, T. Poterba, M. W. Wilson, Y. Tarasova, W. Phu, R. Grant, M. T. Yohannes, Z. Koenig, Y. Farjoun, E. Banks, S. Donnelly, S. Gabriel, N. Gupta, S. Ferriera, C. Tolonen, S. Novod, L. Bergelson, D. Roazen, V. Ruano-Rubio, M. Covarrubias, C. Llanwarne, N. Petrillo, G. Wade, T. Jeandet, R. Munshi, K. Tibbetts, C. Genome Aggregation Database, A. O'Donnell-Luria, M. Solomonson, C. Seed, A. R. Martin, M. E. Talkowski, H. L. Rehm, M. J. Daly, G. Tiao, B. M. Neale, D. G. MacArthur and K. J. Karczewski (2024). "A genomic mutational constraint map using variation in 76,156 human genomes." Nature **625**(7993): 92-100.

Chung, M. K. Y., L. Gong, D. L. Kwong, V. H. Lee, A. W. Lee, X. Y. Guan, N. W. Kam and W. Dai (2023). "Functions of double-negative B cells in autoimmune diseases, infections, and cancers." EMBO Mol Med **15**(9): e17341.

Claussnitzer, M., J. H. Cho, R. Collins, N. J. Cox, E. T. Dermitzakis, M. E. Hurles, S. Kathiresan, E. E. Kenny, C. M. Lindgren, D. G. MacArthur, K. N. North, S. E. Plon, H. L. Rehm, N. Risch, C. N. Rotimi, J. Shendure, N. Soranzo and M. I. McCarthy (2020). "A brief history of human disease genetics." Nature **577**(7789): 179-189.

Consortium, E. P., J. E. Moore, M. J. Purcaro, H. E. Pratt, C. B. Epstein, N. Shoresh, J. Adrian, T. Kawli, C. A. Davis, A. Dobin, R. Kaul, J. Halow, E. L. Van Nostrand, P. Freese, D. U. Gorkin, Y. Shen, Y. He, M. Mackiewicz, F. Pauli-Behn, B. A. Williams, A. Mortazavi, C. A. Keller, X. O. Zhang, S. I. Elhajjajy, J. Huey, D. E. Dickel, V. Snetkova, X. Wei, X. Wang, J. C. Rivera-Mulia, J. Rozowsky, J. Zhang, S. B. Chhetri, J. Zhang, A. Victorsen, K. P. White, A. Visel, G. W. Yeo, C. B. Burge, E. Lecuyer, D. M. Gilbert, J. Dekker, J. Rinn, E. M. Mendenhall, J. R. Ecker, M. Kellis,

R. J. Klein, W. S. Noble, A. Kundaje, R. Guigo, P. J. Farnham, J. M. Cherry, R. M. Myers, B. Ren, B. R. Graveley, M. B. Gerstein, L. A. Pennacchio, M. P. Snyder, B. E. Bernstein, B. Wold, R. C. Hardison, T. R. Gingeras, J. A. Stamatoyannopoulos and Z. Weng (2020). "Expanded encyclopaedias of DNA elements in the human and mouse genomes." Nature **583**(7818): 699-710.

Corces, M. R., A. E. Trevino, E. G. Hamilton, P. G. Greenside, N. A. Sinnott-Armstrong, S. Vesuna, A. T. Satpathy, A. J. Rubin, K. S. Montine, B. Wu, A. Kathiria, S. W. Cho, M. R. Mumbach, A. C. Carter, M. Kasowski, L. A. Orloff, V. I. Risca, A. Kundaje, P. A. Khavari, T. J. Montine, W. J. Greenleaf and H. Y. Chang (2017). "An improved ATAC-seq protocol reduces background and enables interrogation of frozen tissues." Nat Methods **14**(10): 959-962.

Eraslan, G., Z. Avsec, J. Gagneur and F. J. Theis (2019). "Deep learning: new computational modelling techniques for genomics." Nat Rev Genet **20**(7): 389-403.

Fillatreau, S., B. Manfroi and T. Dorner (2021). "Toll-like receptor signalling in B cells during systemic lupus erythematosus." Nat Rev Rheumatol **17**(2): 98-108.

Fulco, C. P., J. Nasser, T. R. Jones, G. Munson, D. T. Bergman, V. Subramanian, S. R. Grossman, R. Anyoha, B. R. Doughty, T. A. Patwardhan, T. H. Nguyen, M. Kane, E. M. Perez, N. C. Durand, C. A. Lareau, E. K. Stamenova, E. L. Aiden, E. S. Lander and J. M. Engreitz (2019). "Activity-by-contact model of enhancer-promoter regulation from thousands of CRISPR perturbations." Nat Genet **51**(12): 1664-1669.

Gate, R. E., C. S. Cheng, A. P. Aiden, A. Siba, M. Tabaka, D. Lituiev, I. Machol, M. G. Gordon, M. Subramaniam, M. Shamim, K. L. Hougen, I. Wortman, S. C. Huang, N. C. Durand, T. Feng, P. L. De Jager, H. Y. Chang, E. L. Aiden, C. Benoist, M. A. Beer, C. J. Ye and A. Regev (2018). "Genetic determinants of co-accessible chromatin regions in activated T cells across humans." Nat Genet **50**(8): 1140-1150.

Gupta, A., K. Weinand, A. Nathan, S. Sakaue, M. J. Zhang, R. A. S. L. E. P. Accelerating Medicines Partnership, Network, L. Donlin, K. Wei, A. L. Price, T. Amariuta and S. Raychaudhuri (2023). "Dynamic regulatory elements in single-cell multimodal data implicate key immune cell states enriched for autoimmune disease heritability." Nat Genet **55**(12): 2200-2210.

Harb, H. and T. A. Chatila (2023). "Regulatory T-cells in asthma." Curr Opin Allergy Clin Immunol **23**(2): 151-157.

Hnisz, D., B. J. Abraham, T. I. Lee, A. Lau, V. Saint-André, A. A. Sigova, H. A. Hoke and R. A. Young (2013). "Super-enhancers in the control of cell identity and disease." Cell **155**(4): 934-947.

Honda, T. and K. Kabashima (2020). "Reconciling innate and acquired immunity in atopic dermatitis." J Allergy Clin Immunol **145**(4): 1136-1137.

Ishigaki, K., S. Sakaue, C. Terao, Y. Luo, K. Sonehara, K. Yamaguchi, T. Amariuta, C. L. Too, V. A. Laufer, I. C. Scott, S. Viatte, M. Takahashi, K. Ohmura, A. Murasawa, M. Hashimoto, H. Ito, M. Hammoudeh, S. A. Emadi, B. K. Masri, H. Halabi, H. Badsha, I. W. Uthman, X. Wu, L. Lin, T. Li, D. Plant, A. Barton, G. Orozco, S. M. M. Verstappen, J. Bowes, A. J. MacGregor, S. Honda, M. Koido, K. Tomizuka, Y. Kamatani, H. Tanaka, E. Tanaka, A. Suzuki, Y. Maeda, K. Yamamoto, S. Miyawaki, G. Xie, J. Zhang, C. I. Amos, E. Keystone, G. Wolbink, I. van der Horst-Bruinsma, J. Cui, K. P. Liao, R. J. Carroll, H. S. Lee, S. Y. Bang, K. A. Siminovitch, N. de Vries, L. Alfredsson, S. Rantapaa-Dahlqvist, E. W. Karlson, S. C. Bae, R. P. Kimberly, J. C. Edberg, X. Mariette, T. Huizinga, P. Dieude, M. Schneider, M. Kerick, J. C. Denny, P. BioBank Japan, K. Matsuda, K. Matsuo, T. Mimori, F. Matsuda, K. Fujio, Y. Tanaka, A. Kumanogoh, M. Traylor, C. M. Lewis, S. Eyre, H. Xu, R. Saxena, T. Arayssi, Y. Kochi, K. Ikari, M. Harigai, P. K. Gregersen, K. Yamamoto, S. Louis Bridges, Jr., L. Padyukov, J. Martin, L. Klareskog, Y. Okada and S. Raychaudhuri (2022). "Multi-ancestry genome-wide association analyses identify novel genetic mechanisms in rheumatoid arthritis." Nat Genet **54**(11): 1640-1651.

Ishikawa, Y., N. Tanaka, Y. Asano, M. Kodera, Y. Shirai, M. Akahoshi, M. Hasegawa, T. Matsushita, K. Saito, S. I. Motegi, H. Yoshifuji, A. Yoshizaki, T. Kohmoto, K. Takagi, A. Oka, M. Kanda, Y. Tanaka, Y. Ito, K. Nakano, H. Kasamatsu, A. Utsunomiya, A. Sekiguchi, H. Niiro, M. Jinnin, K. Makino, T. Makino, H. Ihn, M. Yamamoto, C. Suzuki, H. Takahashi, E. Nishida, A.

Morita, T. Yamamoto, M. Fujimoto, Y. Kondo, D. Goto, T. Sumida, N. Ayuzawa, H. Yanagida, T. Horita, T. Atsumi, H. Endo, Y. Shima, A. Kumanogoh, J. Hirata, N. Otomo, H. Suetsugu, Y. Koike, K. Tomizuka, S. Yoshino, X. Liu, S. Ito, K. Hikino, A. Suzuki, Y. Momozawa, S. Ikegawa, Y. Tanaka, O. Ishikawa, K. Takehara, T. Torii, S. Sato, Y. Okada, T. Mimori, F. Matsuda, K. Matsuda, T. Amariuta, I. Imoto, K. Matsuo, M. Kuwana, Y. Kawaguchi, K. Ohmura and C. Terao (2024). "GWAS for systemic sclerosis identifies six novel susceptibility loci including one in the Fcgamma receptor region." Nat Commun **15**(1): 319.

Jarvinen, T. M., A. Hellquist, M. Zucchelli, S. Koskenmies, J. Panelius, T. Hasan, H. Julkunen, M. D'Amato and J. Kere (2012). "Replication of GWAS-identified systemic lupus erythematosus susceptibility genes affirms B-cell receptor pathway signalling and strengthens the role of IRF5 in disease susceptibility in a Northern European population." Rheumatology (Oxford) **51**(1): 87-92.

Kanai, M., J. C. Ulirsch, J. Karjalainen, M. Kurki, K. J. Karczewski, E. Fauman, Q. S. Wang, H. Jacobs, F. Aguet, K. G. Ardlie, N. Kerimov, K. Alasoo, C. Benner, K. Ishigaki, S. Sakaue, S. Reilly, T. B. J. Project, FinnGen, Y. Kamatani, K. Matsuda, A. Palotie, B. M. Neale, R. Tewhey, P. C. Sabeti, Y. Okada, M. J. Daly and H. K. Finucane (2021). "Insights from complex trait fine-mapping across diverse populations." medRxiv: 2021.2009.2003.21262975.

Karczewski, K. J., L. C. Francioli, G. Tiao, B. B. Cummings, J. Alfoldi, Q. Wang, R. L. Collins, K. M. Laricchia, A. Ganna, D. P. Birnbaum, L. D. Gauthier, H. Brand, M. Solomonson, N. A. Watts, D. Rhodes, M. Singer-Berk, E. M. England, E. G. Seaby, J. A. Kosmicki, R. K. Walters, K. Tashman, Y. Farjoun, E. Banks, T. Poterba, A. Wang, C. Seed, N. Whiffin, J. X. Chong, K. E. Samocha, E. Pierce-Hoffman, Z. Zappala, A. H. O'Donnell-Luria, E. V. Minikel, B. Weisburd, M. Lek, J. S. Ware, C. Vittal, I. M. Armean, L. Bergelson, K. Cibulskis, K. M. Connolly, M. Covarrubias, S. Donnelly, S. Ferriera, S. Gabriel, J. Gentry, N. Gupta, T. Jeandet, D. Kaplan, C. Llanwarne, R. Munshi, S. Novod, N. Petrillo, D. Roazen, V. Ruano-Rubio, A. Saltzman, M. Schleicher, J. Soto, K. Tibbetts, C. Tolonen, G. Wade, M. E. Talkowski, C. Genome Aggregation Database, B. M. Neale, M. J. Daly and D. G. MacArthur (2020). "The mutational constraint spectrum quantified from variation in 141,456 humans." Nature **581**(7809): 434-443.

Klemm, S. L., Z. Shipony and W. J. Greenleaf (2019). "Chromatin accessibility and the regulatory epigenome." Nat Rev Genet **20**(4): 207-220.

Koido, M., C. C. Hon, S. Koyama, H. Kawaji, Y. Murakawa, K. Ishigaki, K. Ito, J. Sese, N. F. Parrish, Y. Kamatani, P. Carninci and C. Terao (2023). "Prediction of the cell-type-specific transcription of non-coding RNAs from genome sequences via machine learning." Nat Biomed Eng **7**(6): 830-844.

Koyama, S., X. Liu, Y. Koike, K. Hikino, M. Koido, W. Li, K. Akaki, K. Tomizuka, S. Ito, N. Otomo, H. Suetsugu, S. Yoshino, M. Akiyama, K. Saito, Y. Ishikawa, C. Benner, P. Natarajan, P. T. Ellinor, T. Mushiroda, M. Horikoshi, M. Ikeda, N. Iwata, K. Matsuda, K. Matsuda, S. Niida, K. Ozaki, Y. Momozawa, S. Ikegawa, O. Takeuchi, K. Ito, C. Terao and P. Biobank Japan (2024). "Population-specific putative causal variants shape quantitative traits." Nature Genetics.

Kuderna, L. F. K., J. C. Ulirsch, S. Rashid, M. Ameen, L. Sundaram, G. Hickey, A. J. Cox, H. Gao, A. Kumar, F. Aguet, M. J. Christmas, H. Clawson, M. Haeussler, M. C. Janiak, M. Kuhlwilm, J. D. Orkin, T. Bataillon, S. Manu, A. Valenzuela, J. Bergman, M. Rouselle, F. E. Silva, L. Agueda, J. Blanc, M. Gut, D. de Vries, I. Goodhead, R. A. Harris, M. Raveendran, A. Jensen, I. S. Chuma, J. E. Horvath, C. Hvilsom, D. Juan, P. Frandsen, J. G. Schraiber, F. R. de Melo, F. Bertuol, H. Byrne, I. Sampaio, I. Farias, J. Valsecchi, M. Messias, M. N. F. da Silva, M. Trivedi, R. Rossi, T. Hrbek, N. Andriaholinirina, C. J. Rabarivola, A. Zaramody, C. J. Jolly, J. Phillips-Conroy, G. Wilkerson, C. Abee, J. H. Simmons, E. Fernandez-Duque, S. Kanthaswamy, F. Shiferaw, D. Wu, L. Zhou, Y. Shao, G. Zhang, J. D. Keyyu, S. Knauf, M. D. Le, E. Lizano, S. Merker, A. Navarro, T. Nadler, C. C. Khor, J. Lee, P. Tan, W. K. Lim, A. C. Kitchener, D. Zinner, I. Gut, A. D. Melin, K. Guschanski, M. H. Schierup, R. M. D. Beck, I. Karakikes, K. C. Wang, G. Umapathy, C. Roos, J. P. Boubli, A. Siepel, A. Kundaje, B. Paten, K. Lindblad-Toh, J. Rogers, T. Marques Bonet and K. K. Farh (2024). "Identification of constrained sequence elements across 239 primate genomes." Nature **625**(7996): 735-742.

Kumasaka, N., A. J. Knights and D. J. Gaffney (2016). "Fine-mapping cellular QTLs with RASQUAL and ATAC-seq." Nat Genet **48**(2): 206-213.
Li, R. and G. Quon (2019). "scBFA: modeling detection patterns to mitigate technical noise in large-scale single-cell genomics data." Genome Biol **20**(1): 193.
Li, Y., Z. Li and F. Hu (2021). "Double-negative (DN) B cells: an under-recognized effector memory B cell subset in autoimmunity." Clin Exp Immunol **205**(2): 119-127.
Li, Y. K., H. Y. Wang, Y. Chen, X. Q. Shi, X. X. Zhang, K. Li, W. P. Fu and C. Sun (2023). "Single‐nucleotide polymorphism rs6592645 confers asthma risk through regulating LRRC32 expression." Exp Ther Med **26**(3): 451.
Liu, X., S. Koyama, K. Tomizuka, S. Takata, Y. Ishikawa, S. Ito, S. Kosugi, K. Suzuki, K. Hikino, M. Koido, Y. Koike, M. Horikoshi, T. Gakuhari, S. Ikegawa, K. Matsuda, Y. Momozawa, K. Ito, Y. Kamatani and C. Terao (2024). "Decoding triancestral origins, archaic introgression, and natural selection in the Japanese population by whole-genome sequencing." Sci Adv **10**(16): eadi8419.
Mantle, D., R. A. Heaton and I. P. Hargreaves (2021). "Coenzyme Q10 and Immune Function: An Overview." Antioxidants (Basel) **10**(5).
Martens, L. D., D. S. Fischer, V. A. Yepez, F. J. Theis and J. Gagneur (2024). "Modeling fragment counts improves single-cell ATAC-seq analysis." Nat Methods **21**(1): 28-31.
Maurano, M. T., R. Humbert, E. Rynes, R. E. Thurman, E. Haugen, H. Wang, A. P. Reynolds, R. Sandstrom, H. Qu, J. Brody, A. Shafer, F. Neri, K. Lee, T. Kutyavin, S. Stehling-Sun, A. K. Johnson, T. K. Canfield, E. Giste, M. Diegel, D. Bates, R. S. Hansen, S. Neph, P. J. Sabo, S. Heimfeld, A. Raubitschek, S. Ziegler, C. Cotsapas, N. Sotoodehnia, I. Glass, S. R. Sunyaev, R. Kaul and J. A. Stamatoyannopoulos (2012). "Systematic localization of common disease-associated variation in regulatory DNA." Science **337**(6099): 1190-1195.
Moser, T., K. Akgun, U. Proschmann, J. Sellner and T. Ziemssen (2020). "The role of TH17 cells in multiple sclerosis: Therapeutic implications." Autoimmun Rev **19**(10): 102647.
Mukherjee, R., P. Kanti Barman, P. Kumar Thatoi, R. Tripathy, B. Kumar Das and B. Ravindran (2015). "Non-Classical monocytes display inflammatory features: Validation in Sepsis and Systemic Lupus Erythematous." Sci Rep **5**: 13886.
Nait Saada, J., G. Kalantzis, D. Shyr, F. Cooper, M. Robinson, A. Gusev and P. F. Palamara (2020). "Identity-by-descent detection across 487,409 British samples reveals fine scale population structure and ultra-rare variant associations." Nat Commun **11**(1): 6130.
Nasser, J., D. T. Bergman, C. P. Fulco, P. Guckelberger, B. R. Doughty, T. A. Patwardhan, T. R. Jones, T. H. Nguyen, J. C. Ulirsch, F. Lekschas, K. Mualim, H. M. Natri, E. M. Weeks, G. Munson, M. Kane, H. Y. Kang, A. Cui, J. P. Ray, T. M. Eisenhaure, R. L. Collins, K. Dey, H. Pfister, A. L. Price, C. B. Epstein, A. Kundaje, R. J. Xavier, M. J. Daly, H. Huang, H. K. Finucane, N. Hacohen, E. S. Lander and J. M. Engreitz (2021). "Genome-wide enhancer maps link risk variants to disease genes." Nature **593**(7858): 238-243.
Nassir, N., R. Tambi, A. Bankapur, S. Al Heialy, N. Karuvantevida, H. H. Khansaheb, B. Zehra, G. Begum, R. A. Hameid, A. Ahmed, Z. Deesi, A. Alkhajeh, K. M. F. Uddin, H. Akter, S. A. Safizadeh Shabestari, O. Almidani, A. Islam, M. Gaudet, R. K. Kandasamy, T. Loney, A. A. Tayoun, N. Nowotny, M. Woodbury-Smith, P. Rahman, W. M. Kuebler, M. Yaseen Hachim, J. L. Casanova, B. K. Berdiev, A. Alsheikh-Ali and M. Uddin (2021). "Single-cell transcriptome identifies FCGR3B upregulated subtype of alveolar macrophages in patients with critical COVID-19." iScience **24**(9): 103030.
Nelson, R. K., A. Bush, J. Stokes, P. Nair and P. Akuthota (2020). "Eosinophilic Asthma." J Allergy Clin Immunol Pract **8**(2): 465-473.
Oguchi, A., A. Suzuki, S. Komatsu, H. Yoshitomi, S. Bhagat, R. Son, R. J. P. Bonnal, S. Kojima, M. Koido, K. Takeuchi, K. Myouzen, G. Inoue, T. Hirai, H. Sano, Y. Takegami, A. Kanemaru, I. Yamaguchi, Y. Ishikawa, N. Tanaka, S. Hirabayashi, R. Konishi, S. Sekito, T. Inoue, J. Kere, S. Takeda, A. Takaori-Kondo, I. Endo, S. Kawaoka, H. Kawaji, K. Ishigaki, H. Ueno, Y. Hayashizaki, M. Pagani, P. Carninci, M. Yanagita, I. C. dagger, N. Parrish, C. Terao, K. Yamamoto, Y. Murakawa and I. C. Members (2024). "An atlas of transcribed enhancers across helper T cell diversity for decoding human diseases." Science **385**(6704): eadd8394.

Pollard, K. S., M. J. Hubisz, K. R. Rosenbloom and A. Siepel (2010). "Detection of nonneutral substitution rates on mammalian phylogenies." Genome Res **20**(1): 110-121.

Roadmap Epigenomics, C., A. Kundaje, W. Meuleman, J. Ernst, M. Bilenky, A. Yen, A. Heravi-Moussavi, P. Kheradpour, Z. Zhang, J. Wang, M. J. Ziller, V. Amin, J. W. Whitaker, M. D. Schultz, L. D. Ward, A. Sarkar, G. Quon, R. S. Sandstrom, M. L. Eaton, Y. C. Wu, A. R. Pfenning, X. Wang, M. Claussnitzer, Y. Liu, C. Coarfa, R. A. Harris, N. Shoresh, C. B. Epstein, E. Gjoneska, D. Leung, W. Xie, R. D. Hawkins, R. Lister, C. Hong, P. Gascard, A. J. Mungall, R. Moore, E. Chuah, A. Tam, T. K. Canfield, R. S. Hansen, R. Kaul, P. J. Sabo, M. S. Bansal, A. Carles, J. R. Dixon, K. H. Farh, S. Feizi, R. Karlic, A. R. Kim, A. Kulkarni, D. Li, R. Lowdon, G. Elliott, T. R. Mercer, S. J. Neph, V. Onuchic, P. Polak, N. Rajagopal, P. Ray, R. C. Sallari, K. T. Siebenthall, N. A. Sinnott-Armstrong, M. Stevens, R. E. Thurman, J. Wu, B. Zhang, X. Zhou, A. E. Beaudet, L. A. Boyer, P. L. De Jager, P. J. Farnham, S. J. Fisher, D. Haussler, S. J. Jones, W. Li, M. A. Marra, M. T. McManus, S. Sunyaev, J. A. Thomson, T. D. Tlsty, L. H. Tsai, W. Wang, R. A. Waterland, M. Q. Zhang, L. H. Chadwick, B. E. Bernstein, J. F. Costello, J. R. Ecker, M. Hirst, A. Meissner, A. Milosavljevic, B. Ren, J. A. Stamatoyannopoulos, T. Wang and M. Kellis (2015). "Integrative analysis of 111 reference human epigenomes." Nature **518**(7539): 317-330.

Schaid, D. J., W. Chen and N. B. Larson (2018). "From genome-wide associations to candidate causal variants by statistical fine-mapping." Nat Rev Genet **19**(8): 491-504.

Silvert, M., L. Quintana-Murci and M. Rotival (2019). "Impact and Evolutionary Determinants of Neanderthal Introgression on Transcriptional and Post-Transcriptional Regulation." Am J Hum Genet **104**(6): 1241-1250.

Soskic, B., E. Cano-Gamez, D. J. Smyth, W. C. Rowan, N. Nakic, J. Esparza-Gordillo, L. Bossini-Castillo, D. F. Tough, C. G. C. Larminie, P. G. Bronson, D. Wille and G. Trynka (2019). "Chromatin activity at GWAS loci identifies T cell states driving complex immune diseases." Nat Genet **51**(10): 1486-1493.

Storey, J. D. (2002). "A Direct Approach to False Discovery Rates." Journal of the Royal Statistical Society Series B: Statistical Methodology **64**(3): 479-498.

Tanaka, N., M. Koido, A. Suzuki, N. Otomo, H. Suetsugu, Y. Kochi, K. Tomizuka, Y. Momozawa, Y. Kamatani, P. Biobank Japan, S. Ikegawa, K. Yamamoto and C. Terao (2021). "Eight novel susceptibility loci and putative causal variants in atopic dermatitis." J Allergy Clin Immunol **148**(5): 1293-1306.

Tashman, K. C., R. Cui, L. J. O'Connor, B. M. Neale and H. K. Finucane (2021). "Significance testing for small annotations in stratified LD-Score regression." medRxiv: 2021.2003.2013.21249938.

Terao, C., H. Yoshifuji, T. Matsumura, T. K. Naruse, T. Ishii, Y. Nakaoka, Y. Kirino, K. Matsuo, T. Origuchi, M. Shimizu, Y. Maejima, E. Amiya, N. Tamura, T. Kawaguchi, M. Takahashi, K. Setoh, K. Ohmura, R. Watanabe, T. Horita, T. Atsumi, M. Matsukura, T. Miyata, Y. Kochi, T. Suda, K. Tanemoto, A. Meguro, Y. Okada, A. Ogimoto, M. Yamamoto, H. Takahashi, S. Nakayamada, K. Saito, M. Kuwana, N. Mizuki, Y. Tabara, A. Ueda, I. Komuro, A. Kimura, M. Isobe, T. Mimori and F. Matsuda (2018). "Genetic determinants and an epistasis of LILRA3 and HLA-B*52 in Takayasu arteritis." Proc Natl Acad Sci U S A **115**(51): 13045-13050.

Thibodeau, A., A. Uyar, S. Khetan, M. L. Stitzel and D. Ucar (2018). "A neural network based model effectively predicts enhancers from clinical ATAC-seq samples." Sci Rep **8**(1): 16048.

Tran, D. Q., J. Andersson, R. Wang, H. Ramsey, D. Unutmaz and E. M. Shevach (2009). "GARP (LRRC32) is essential for the surface expression of latent TGF-beta on platelets and activated FOXP3+ regulatory T cells." Proc Natl Acad Sci U S A **106**(32): 13445-13450.

Trynka, G., C. Sandor, B. Han, H. Xu, B. E. Stranger, X. S. Liu and S. Raychaudhuri (2013). "Chromatin marks identify critical cell types for fine mapping complex trait variants." Nat Genet **45**(2): 124-130.

Visscher, P. M., N. R. Wray, Q. Zhang, P. Sklar, M. I. McCarthy, M. A. Brown and J. Yang (2017). "10 Years of GWAS Discovery: Biology, Function, and Translation." Am J Hum Genet **101**(1): 5-22.

Yan, F., D. R. Powell, D. J. Curtis and N. C. Wong (2020). "From reads to insight: a hitchhiker's guide to ATAC-seq data analysis." Genome Biol **21**(1): 22.

Yin, X., K. Kim, H. Suetsugu, S. Y. Bang, L. Wen, M. Koido, E. Ha, L. Liu, Y. Sakamoto, S. Jo, R. X. Leng, N. Otomo, V. Laurynenka, Y. C. Kwon, Y. Sheng, N. Sugano, M. Y. Hwang, W. Li, M. Mukai, K. Yoon, M. Cai, K. Ishigaki, W. T. Chung, H. Huang, D. Takahashi, S. S. Lee, M. Wang, K. Karino, S. C. Shim, X. Zheng, T. Miyamura, Y. M. Kang, D. Ye, J. Nakamura, C. H. Suh, Y. Tang, G. Motomura, Y. B. Park, H. Ding, T. Kuroda, J. Y. Choe, C. Li, H. Niiro, Y. Park, C. Shen, T. Miyamoto, G. Y. Ahn, W. Fei, T. Takeuchi, J. M. Shin, K. Li, Y. Kawaguchi, Y. K. Lee, Y. Wang, K. Amano, D. J. Park, W. Yang, Y. Tada, K. Yamaji, M. Shimizu, T. Atsumi, A. Suzuki, T. Sumida, Y. Okada, K. Matsuda, K. Matsuo, Y. Kochi, H. Japanese Research Committee on Idiopathic Osteonecrosis of the Femoral, L. C. Kottyan, M. T. Weirauch, S. Parameswaran, S. Eswar, H. Salim, X. Chen, K. Yamamoto, J. B. Harley, K. Ohmura, T. H. Kim, S. Yang, T. Yamamoto, B. J. Kim, N. Shen, S. Ikegawa, H. S. Lee, X. Zhang, C. Terao, Y. Cui and S. C. Bae (2021). "Meta-analysis of 208370 East Asians identifies 113 susceptibility loci for systemic lupus erythematosus." Ann Rheum Dis **80**(5): 632-640.

Yuan, H. and D. R. Kelley (2022). "scBasset: sequence-based modeling of single-cell ATAC-seq using convolutional neural networks." Nat Methods **19**(9): 1088-1096.

Zeng, B., J. Bendl, C. Deng, D. Lee, R. Misir, S. M. Reach, S. P. Kleopoulos, P. Auluck, S. Marenco, D. A. Lewis, V. Haroutunian, N. Ahituv, J. F. Fullard, G. E. Hoffman and P. Roussos (2024). "Genetic regulation of cell type-specific chromatin accessibility shapes brain disease etiology." Science **384**(6698): eadh4265.

Zhang, J. Y., X. M. Wang, X. Xing, Z. Xu, C. Zhang, J. W. Song, X. Fan, P. Xia, J. L. Fu, S. Y. Wang, R. N. Xu, X. P. Dai, L. Shi, L. Huang, T. J. Jiang, M. Shi, Y. Zhang, A. Zumla, M. Maeurer, F. Bai and F. S. Wang (2020). "Single-cell landscape of immunological responses in patients with COVID-19." Nat Immunol **21**(9): 1107-1118.

Zhou, J., C. L. Theesfeld, K. Yao, K. M. Chen, A. K. Wong and O. G. Troyanskaya (2018). "Deep learning sequence-based ab initio prediction of variant effects on expression and disease risk." Nat Genet **50**(8): 1171-1179.

Zhou, J. and O. G. Troyanskaya (2015). "Predicting effects of noncoding variants with deep learning-based sequence model." Nat Methods **12**(10): 931-934.

Figure 1 | Study design

A

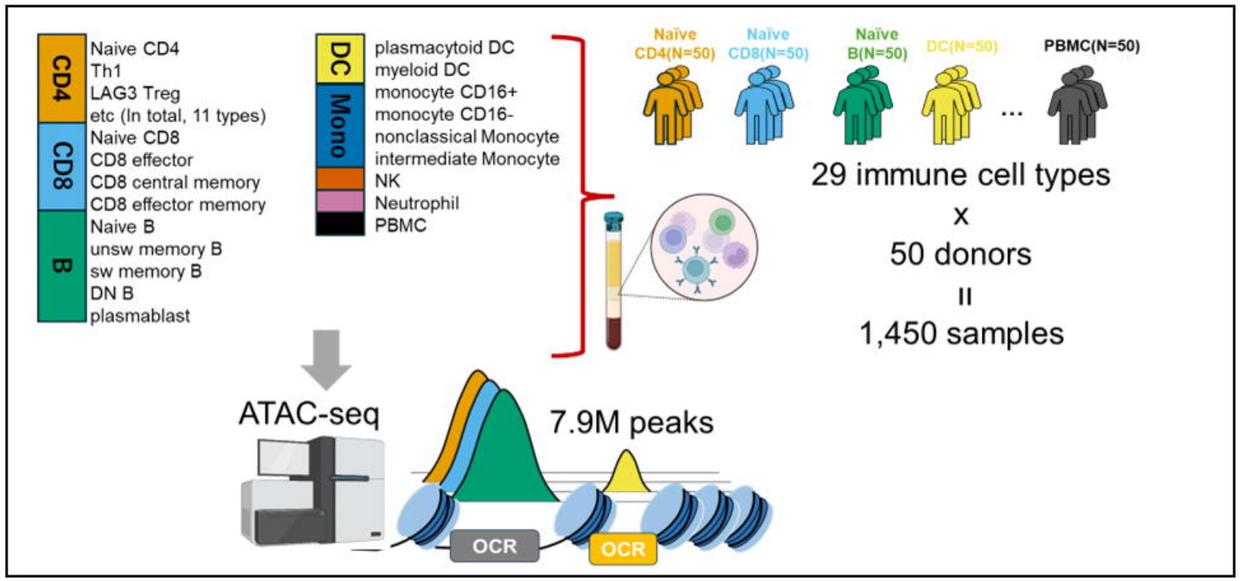

C

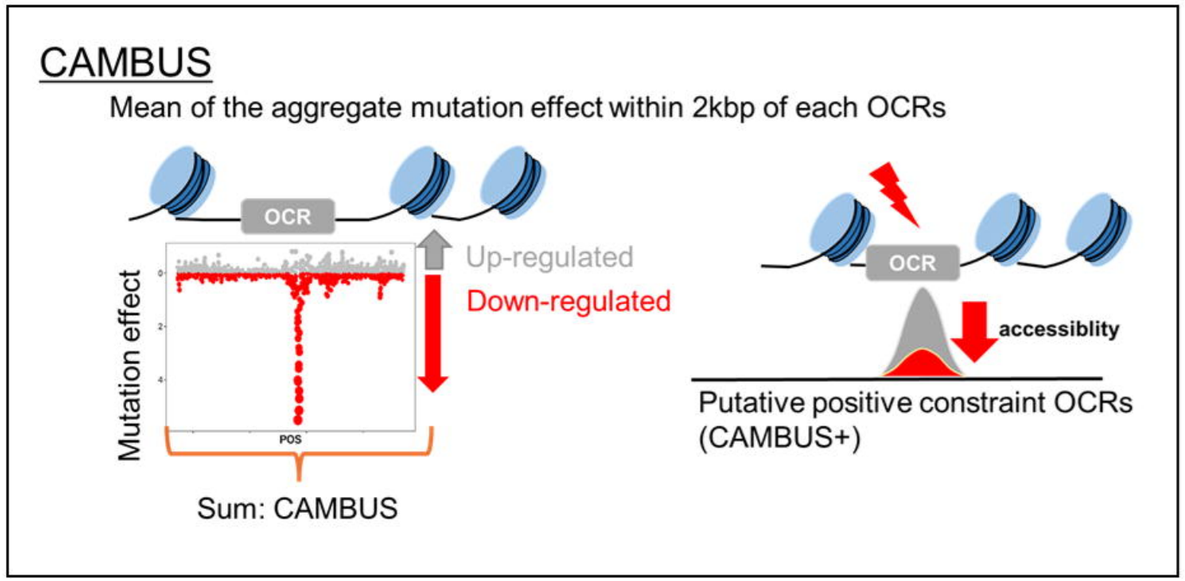

B

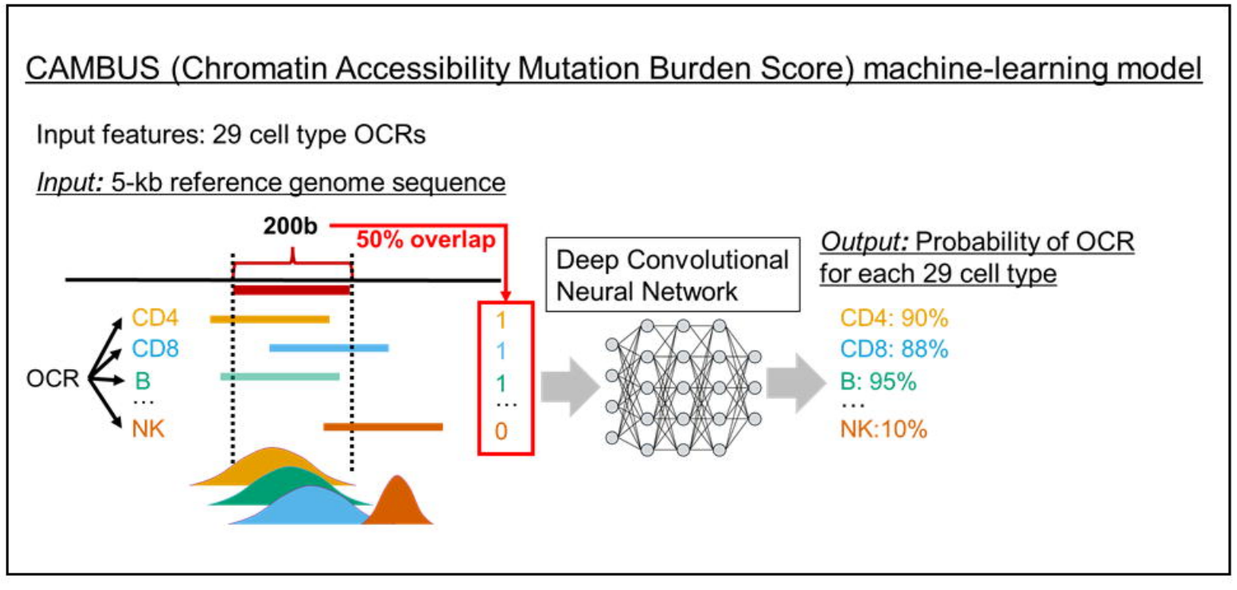

D

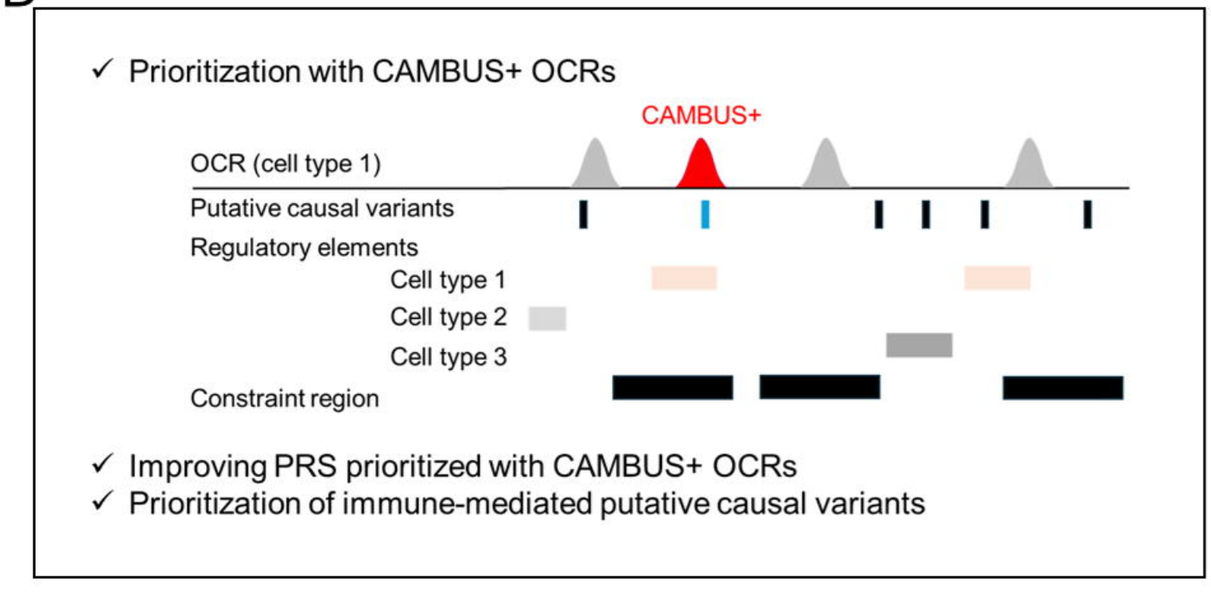

Created with biorender.com

Figure 2 | Accuracy of mutation effect for CAMBUS ML model

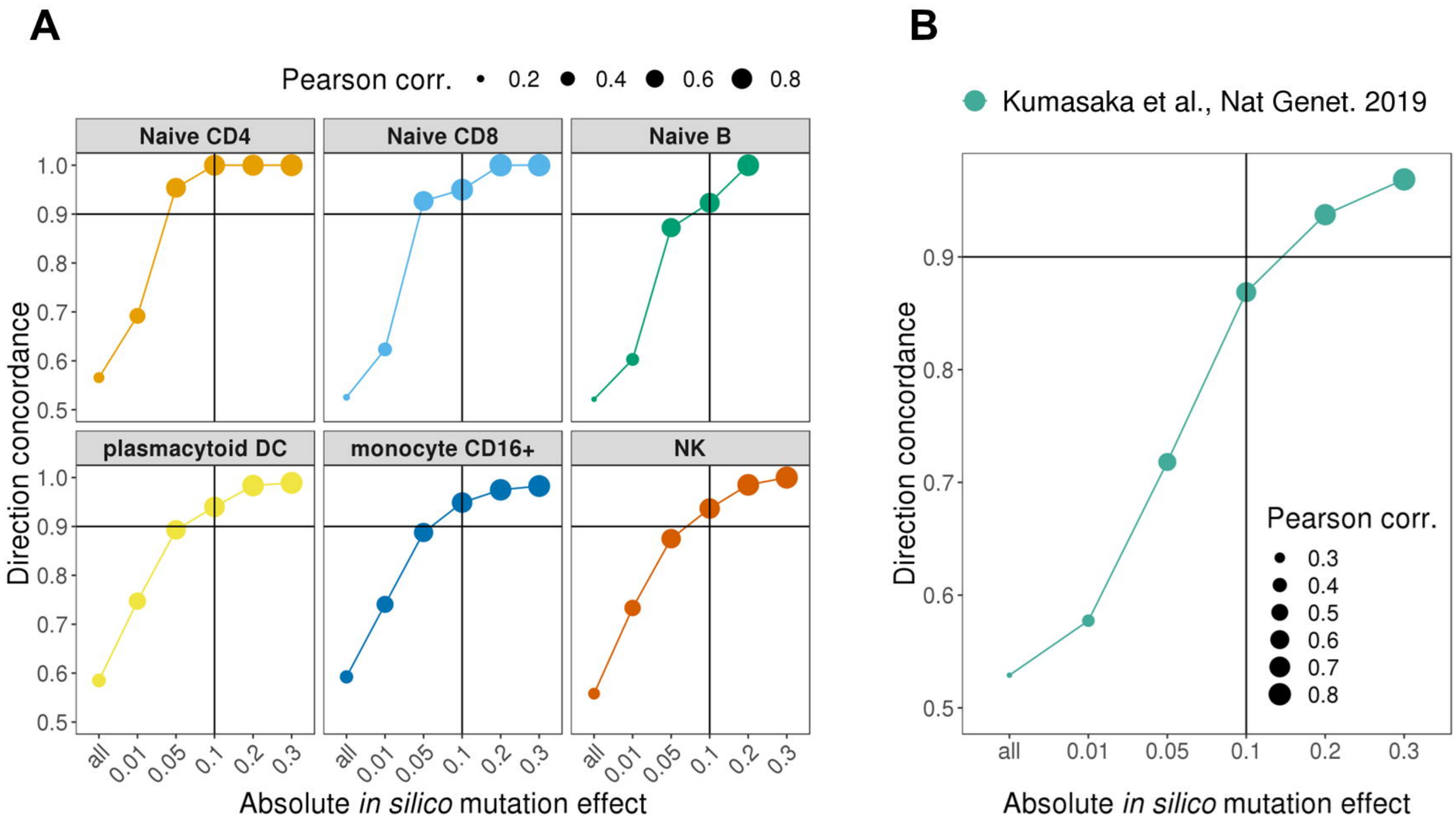

Figure 3 | CAMBUS+ OCRs can mark constraint regions and active enhancers

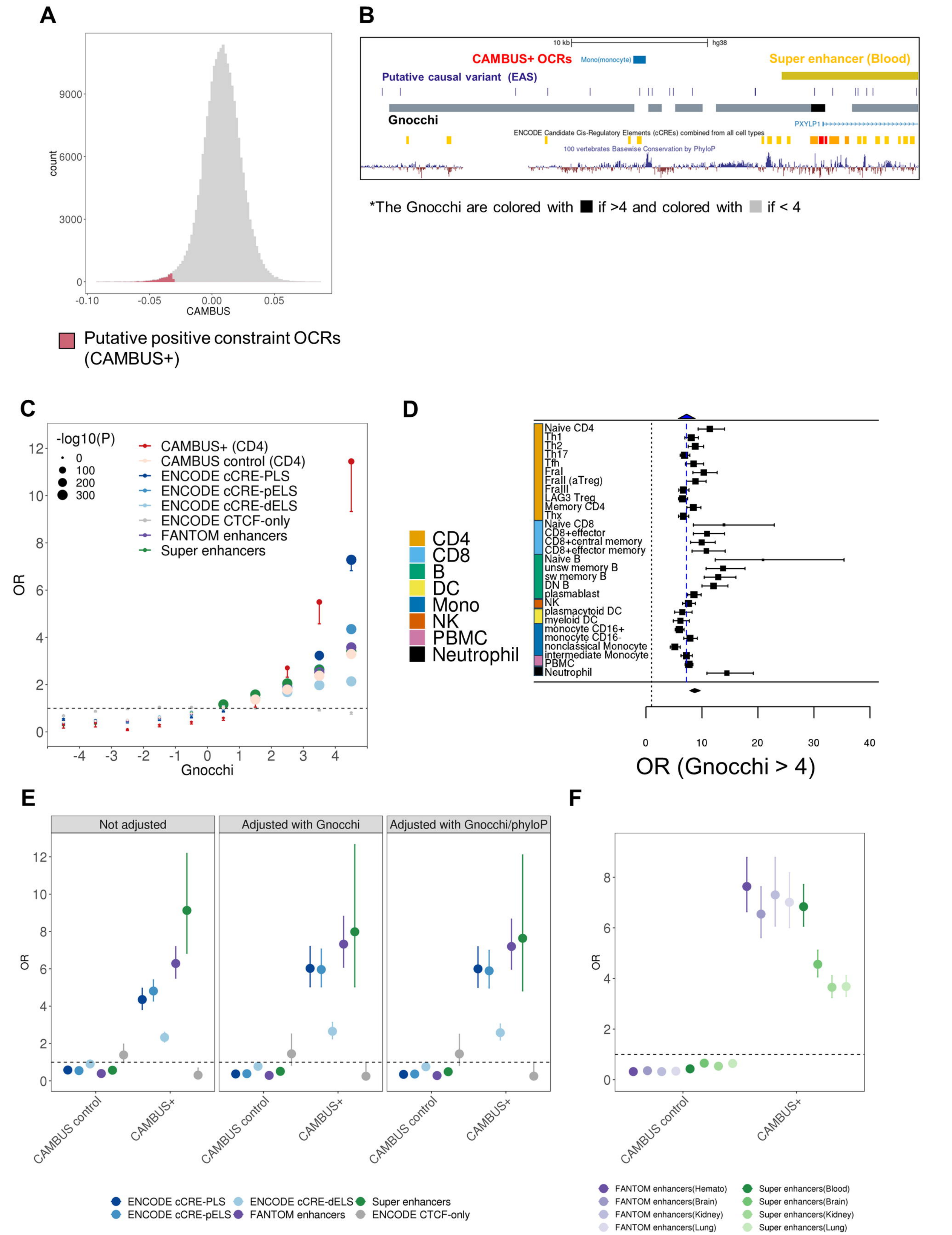

Figure 4 | Heritability enrichment for immune-mediated diseases

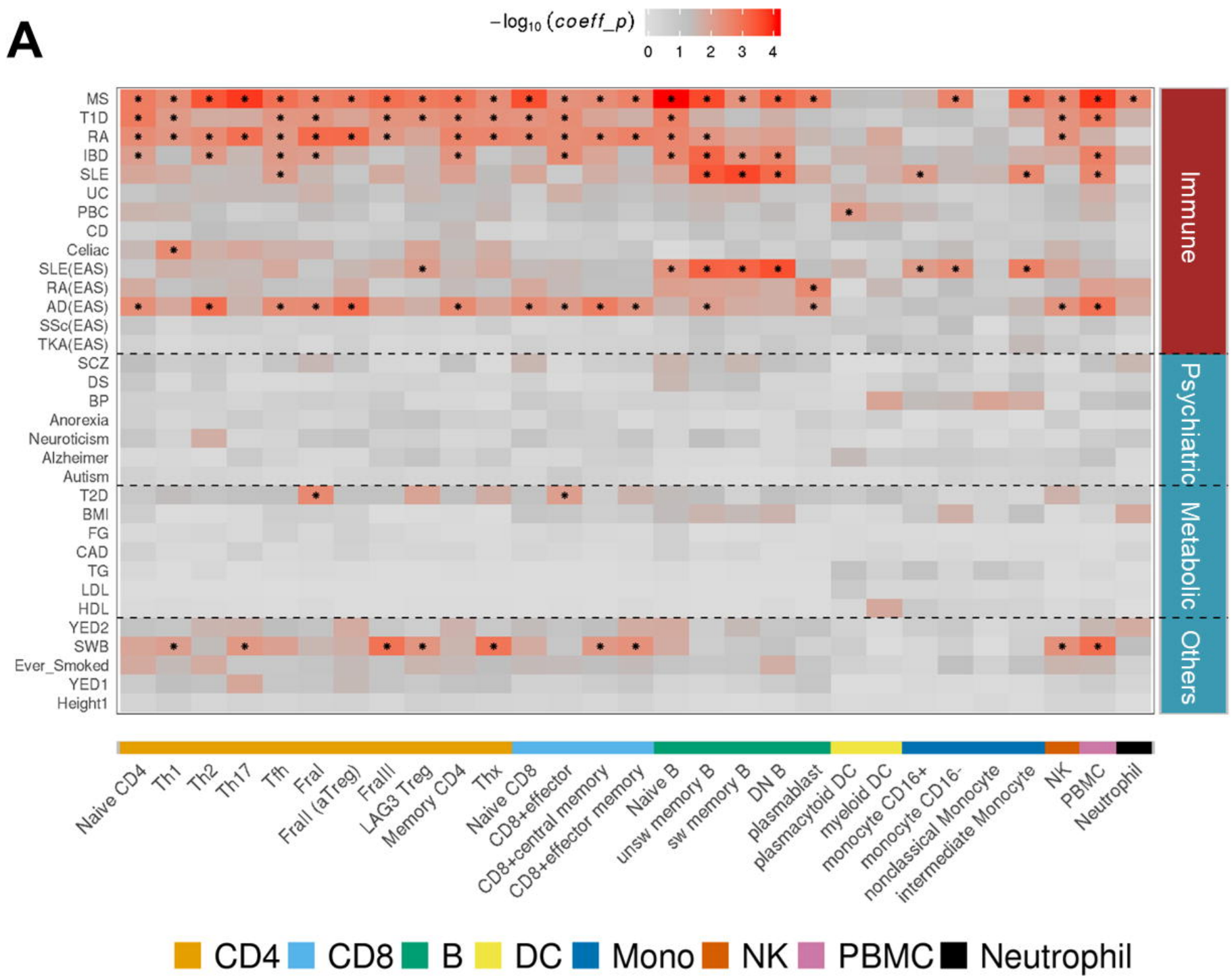

Figure 5 | Enrichment analysis for fine-mapped variants in CAMBUS+ OCRs

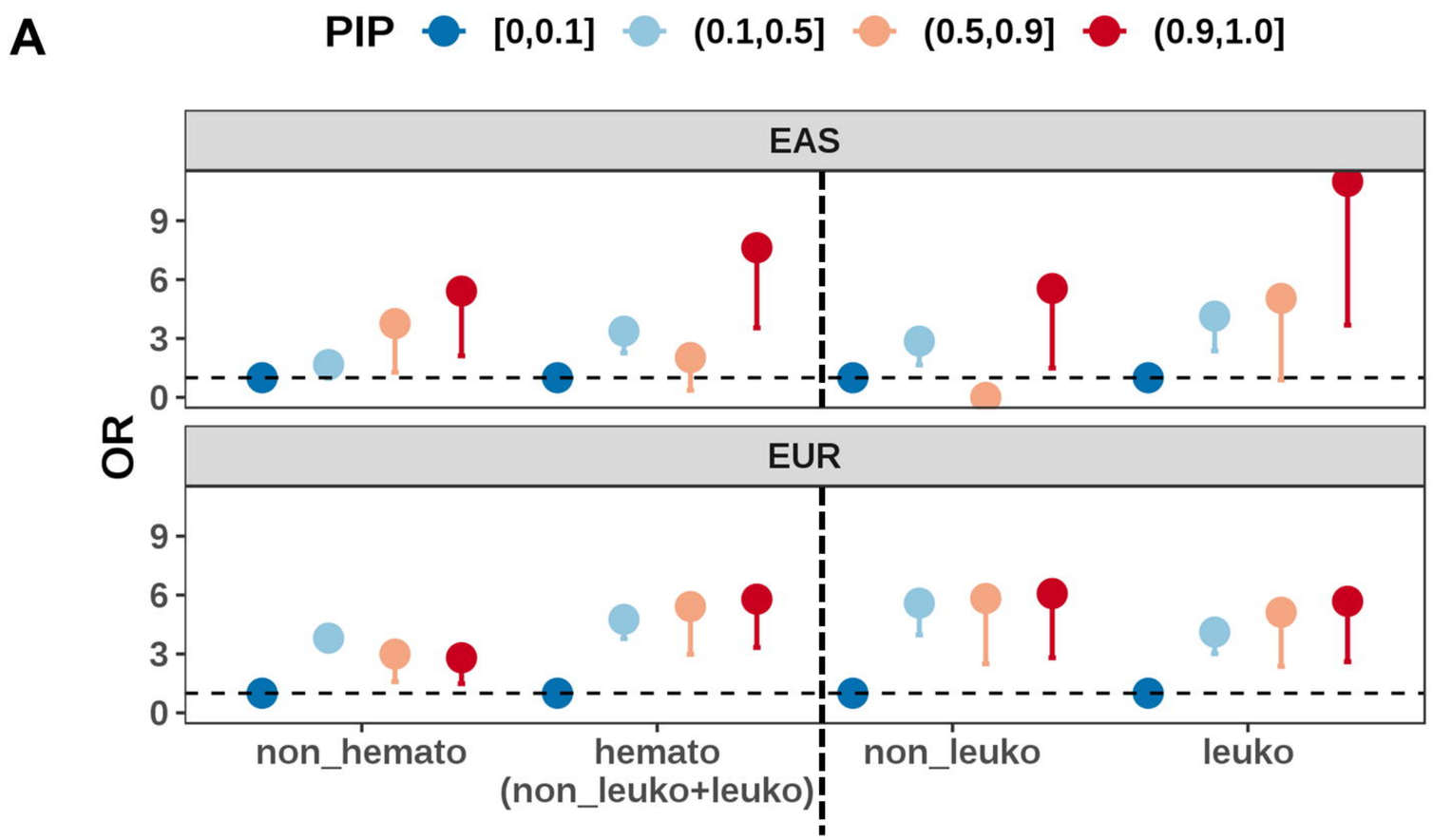

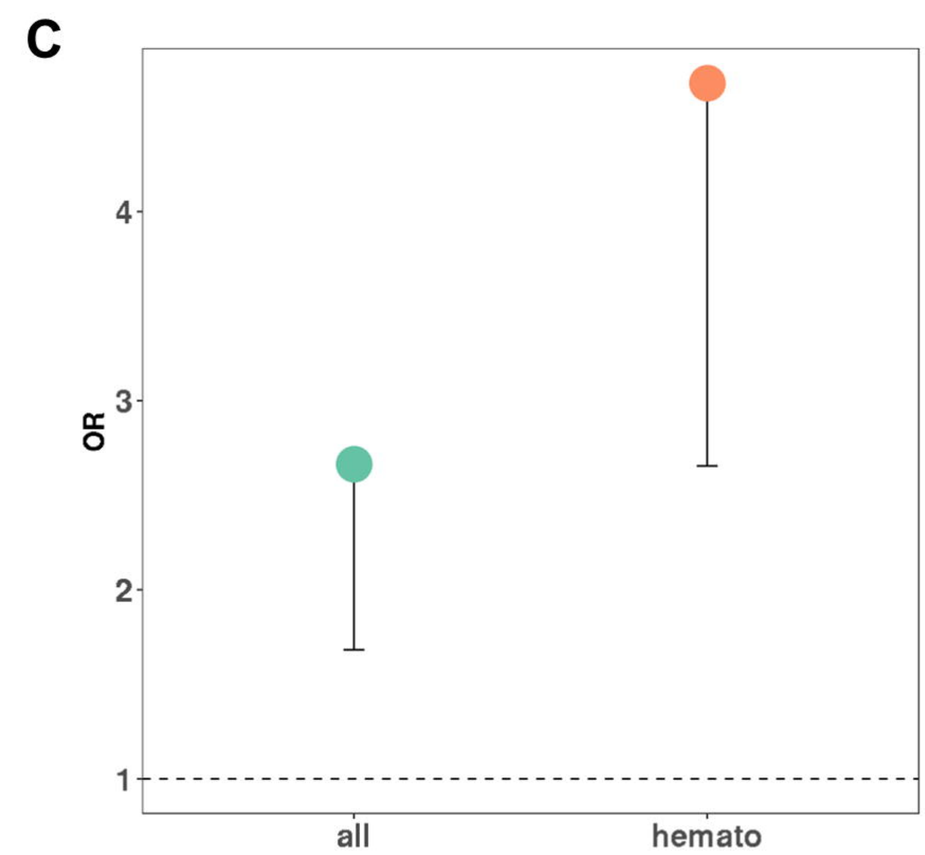

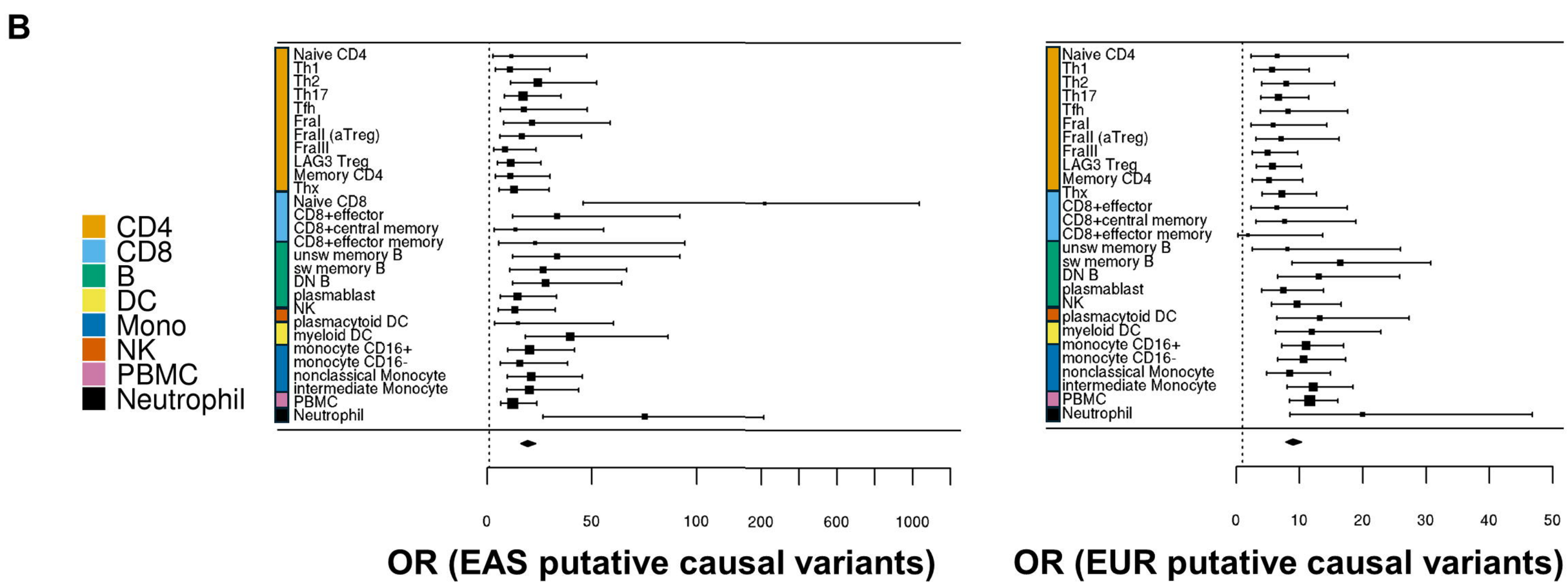

Figure 6 | Prioritization of the putative causal variants using CAMBUS+ OCRs

A

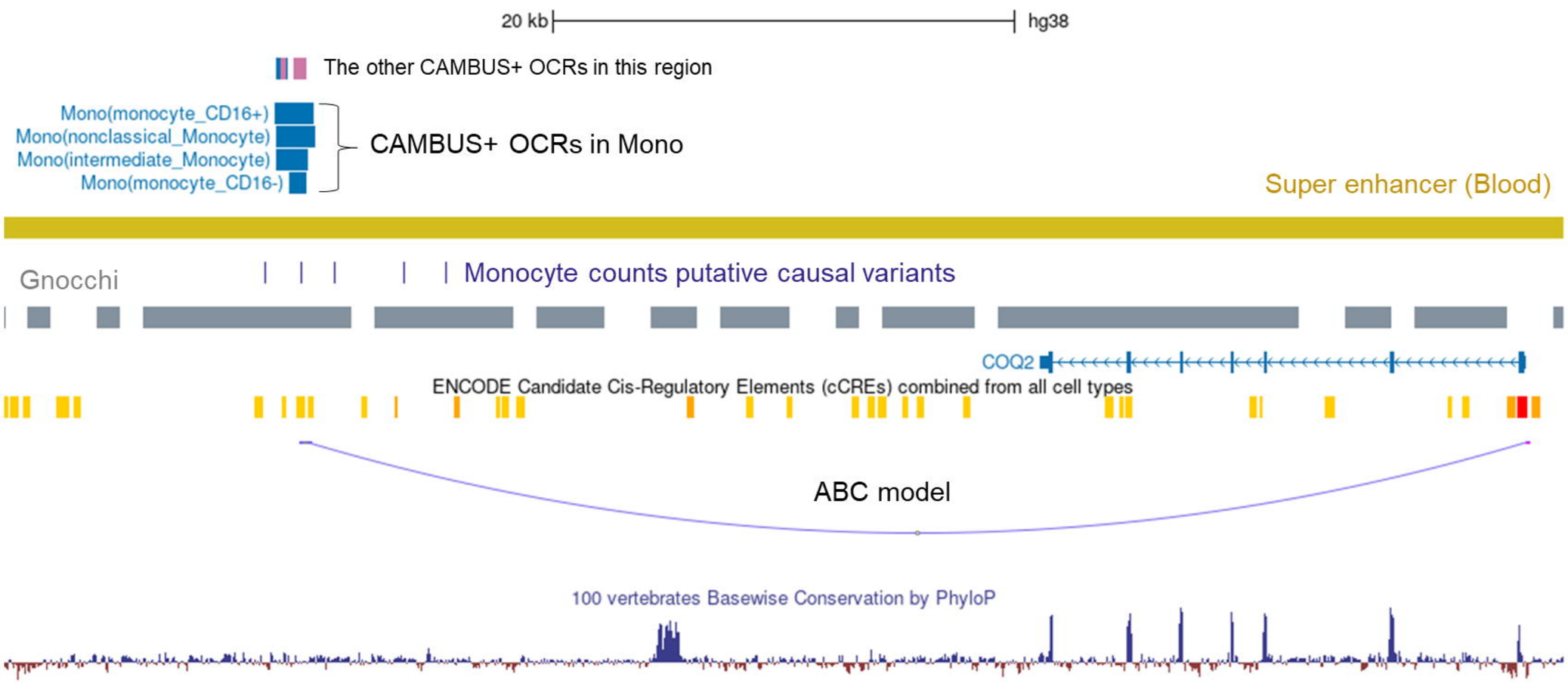

B

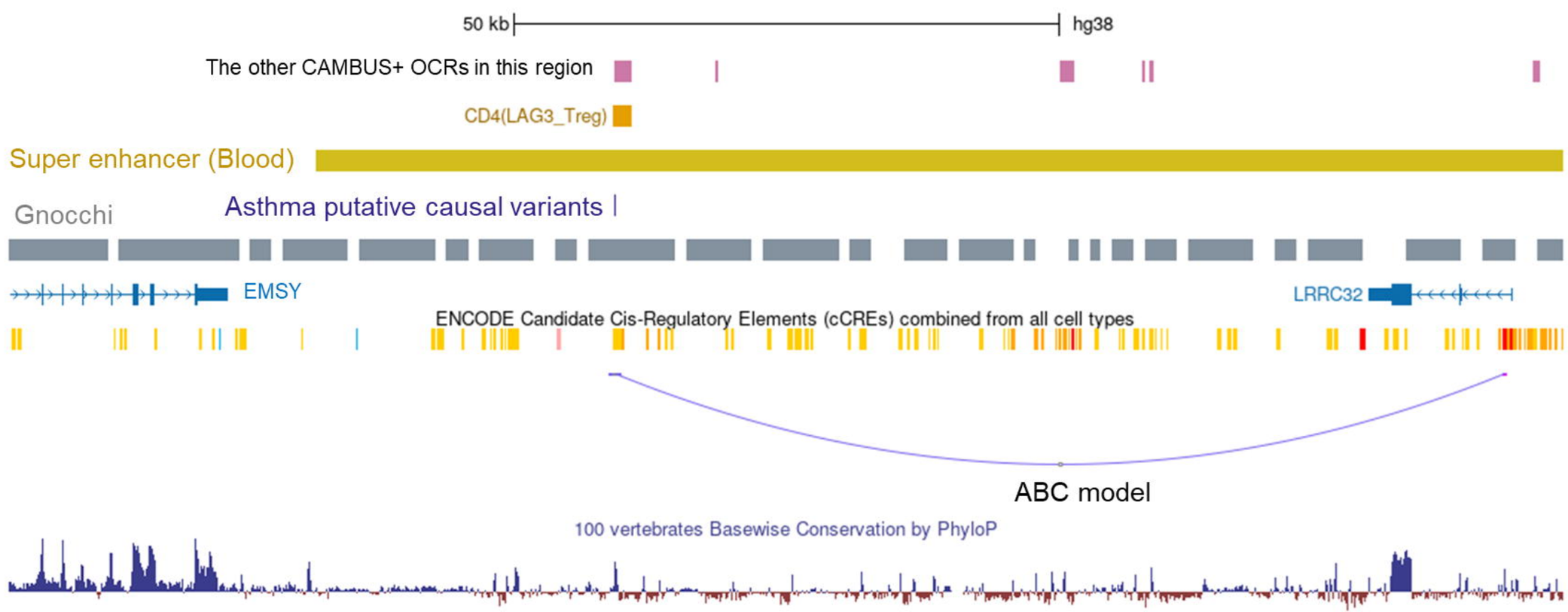

Figure S1 | Clustering analysis and PCA/umap

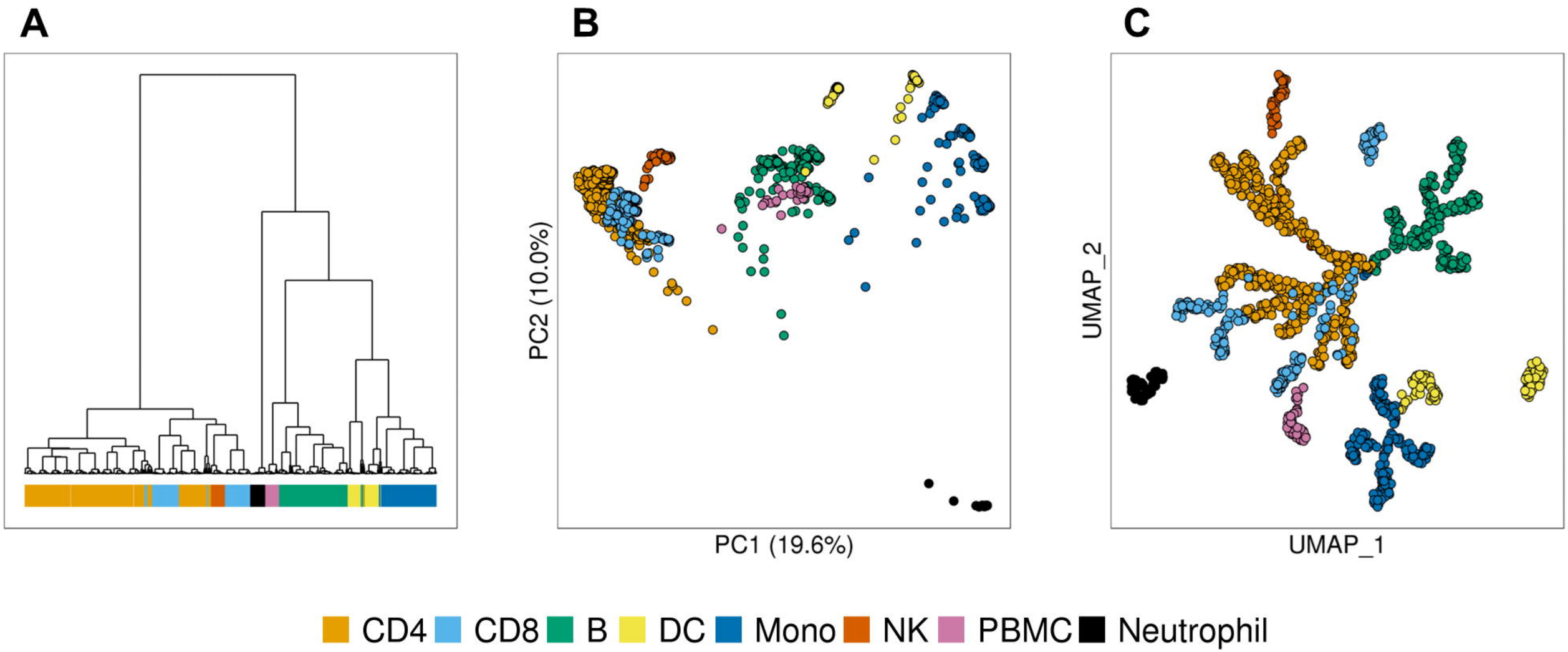

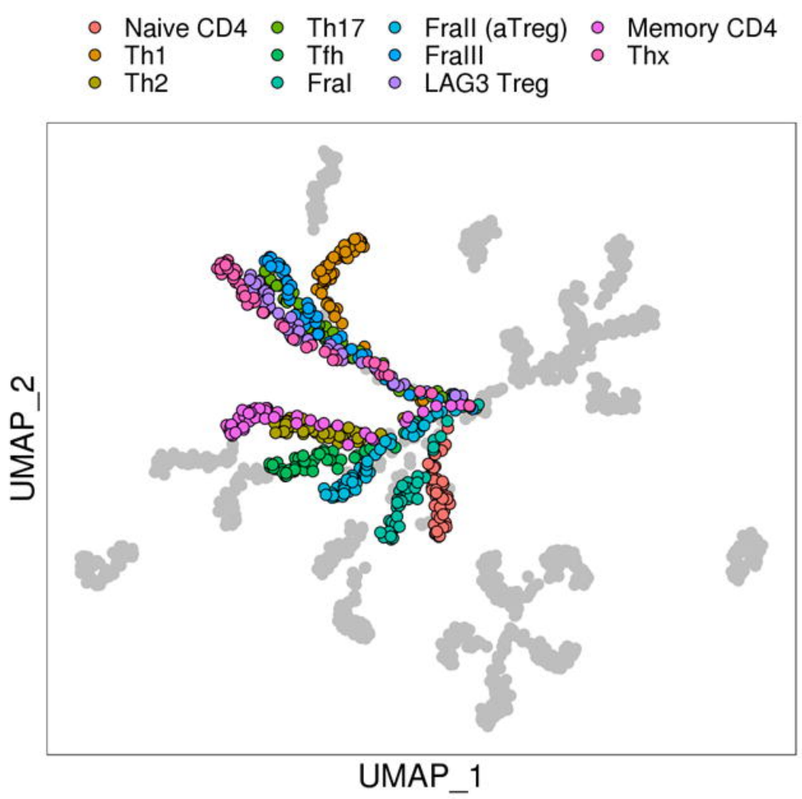

Figure S2 | Accuracy of CAMBUS ML model

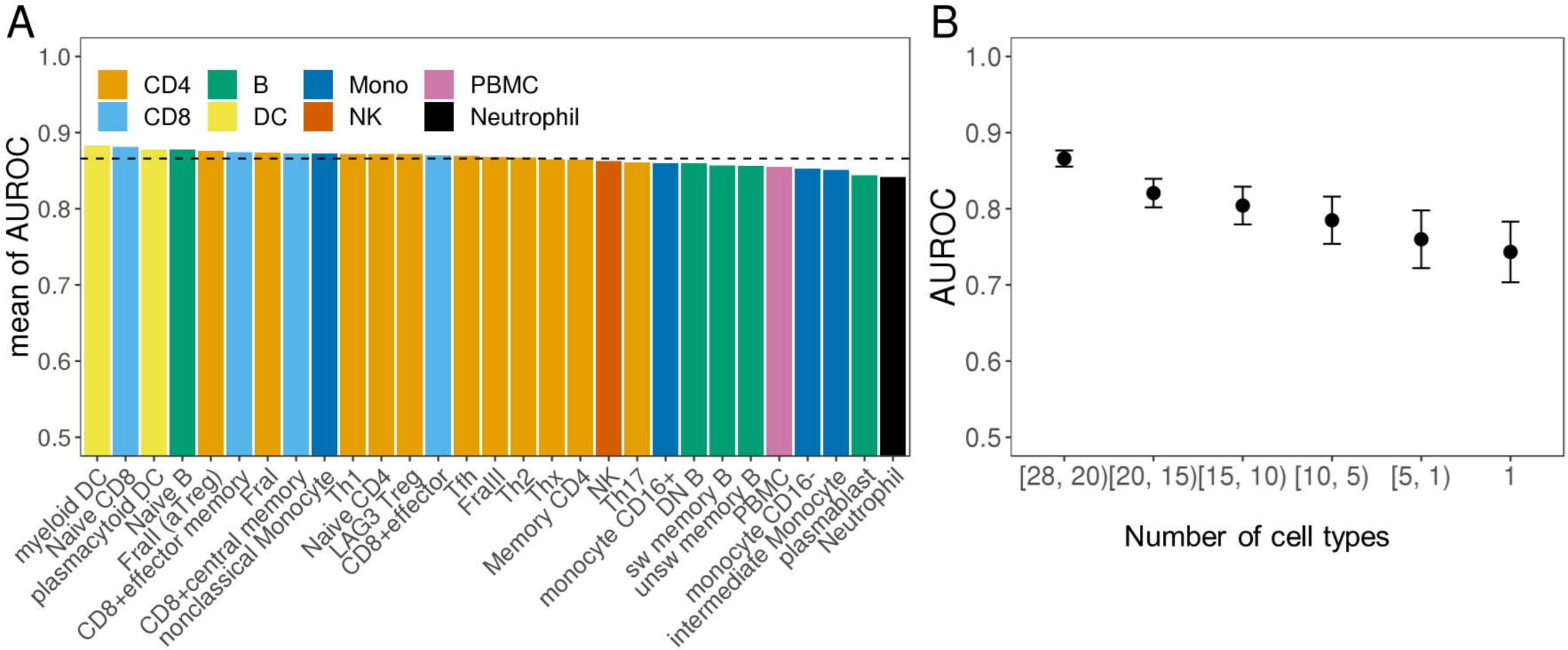

Figure S3 | Accuracy of CAMBUS ML model

A

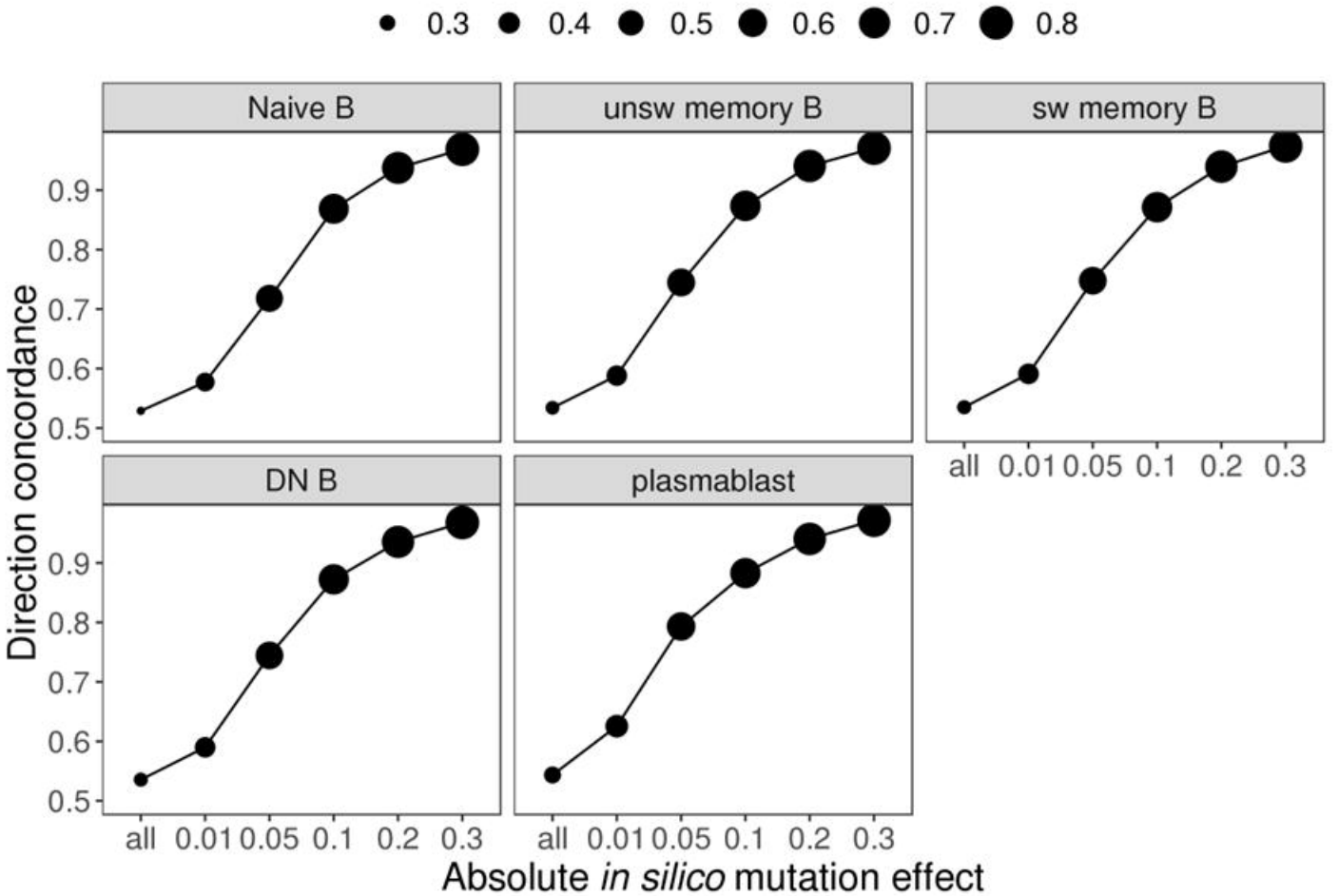

B

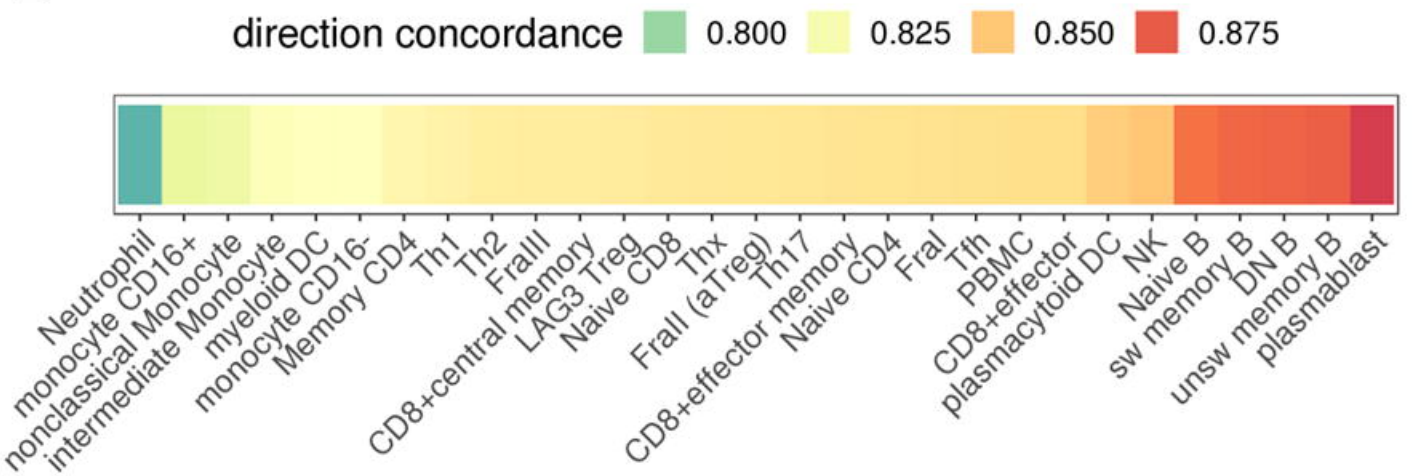

Figure S4 | CAMBUS+ OCRs can mark constraint regions and active enhancers

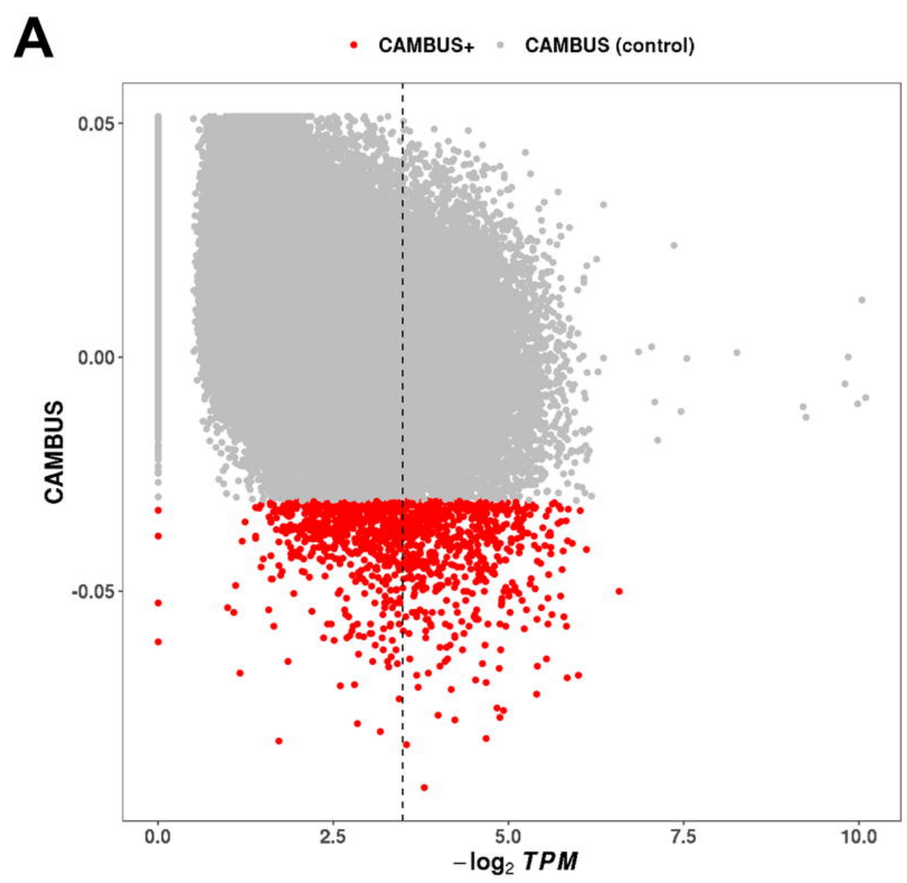

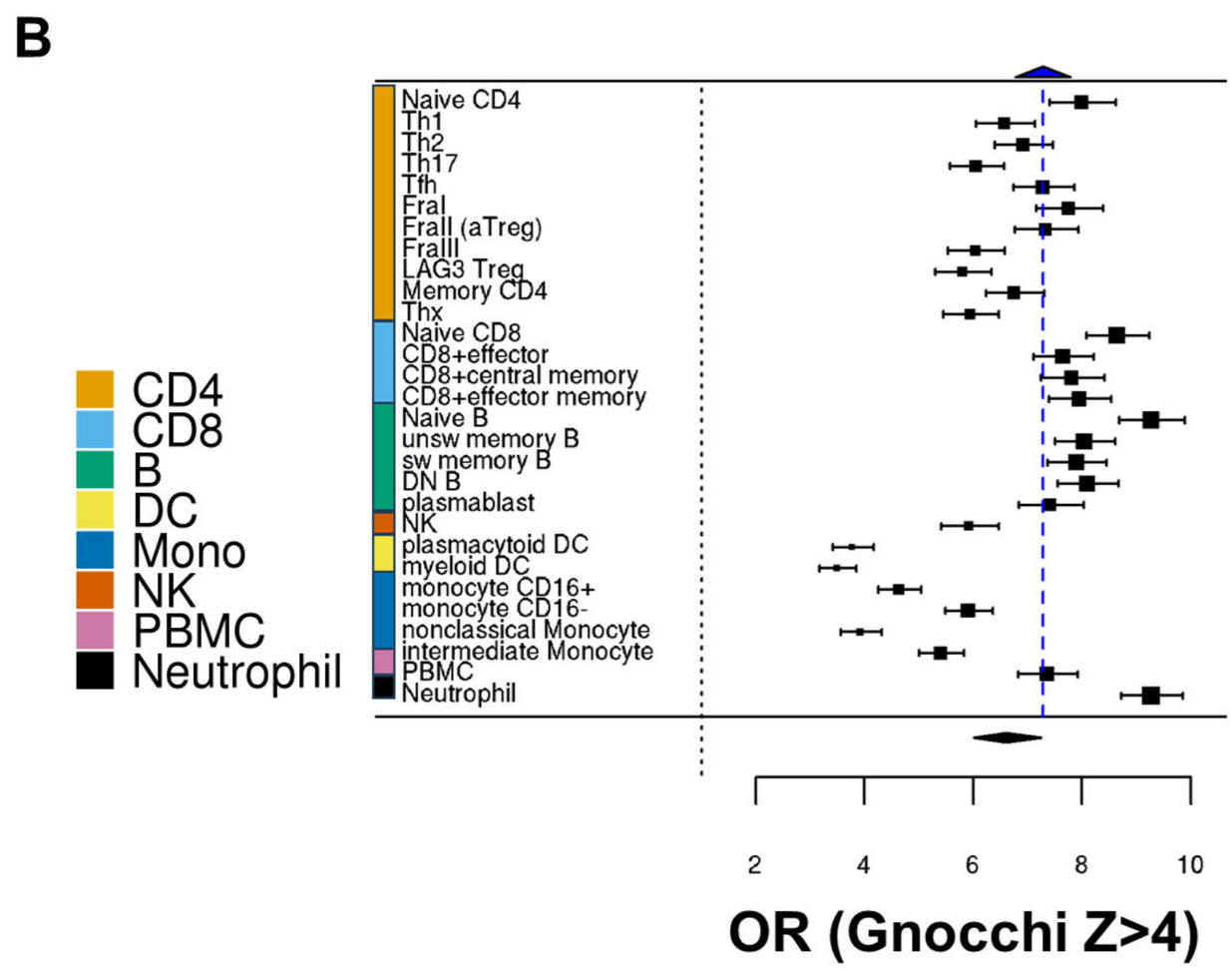

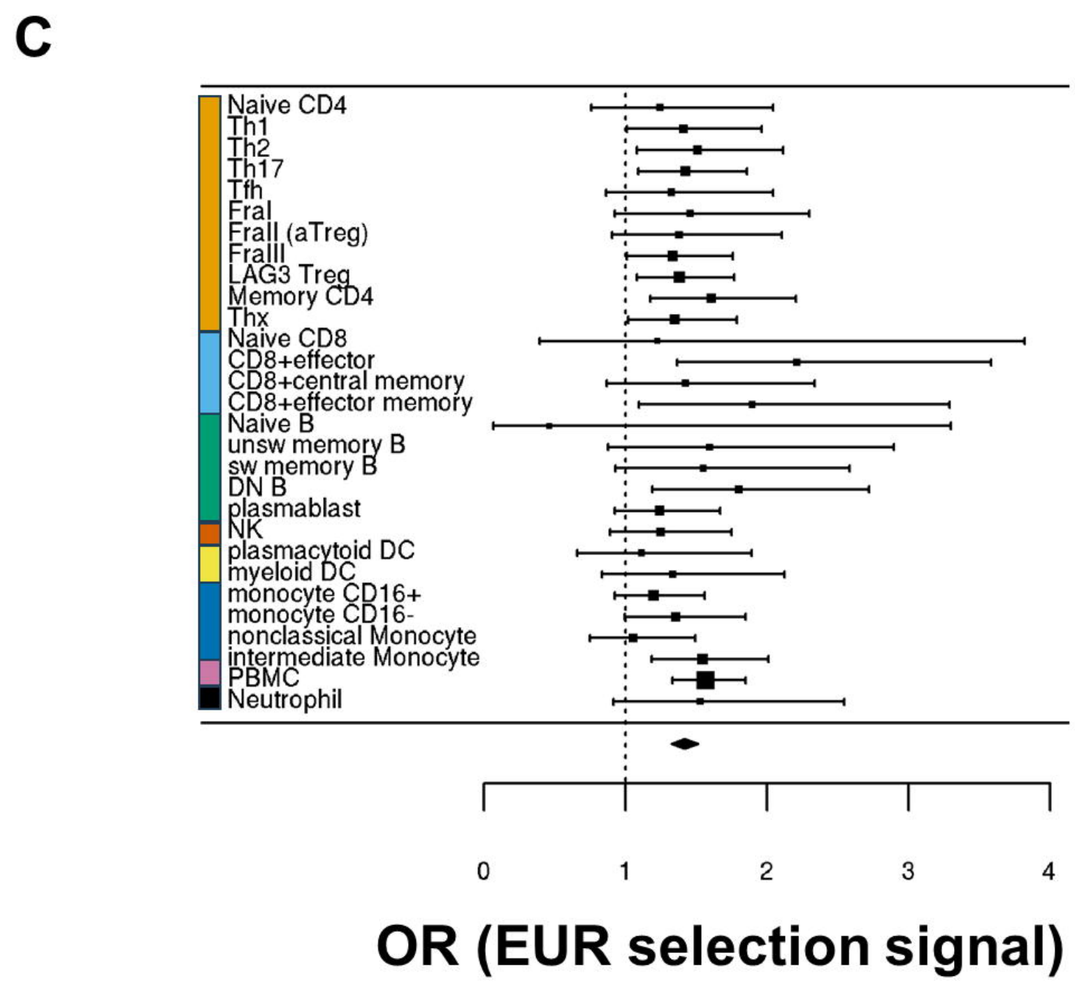

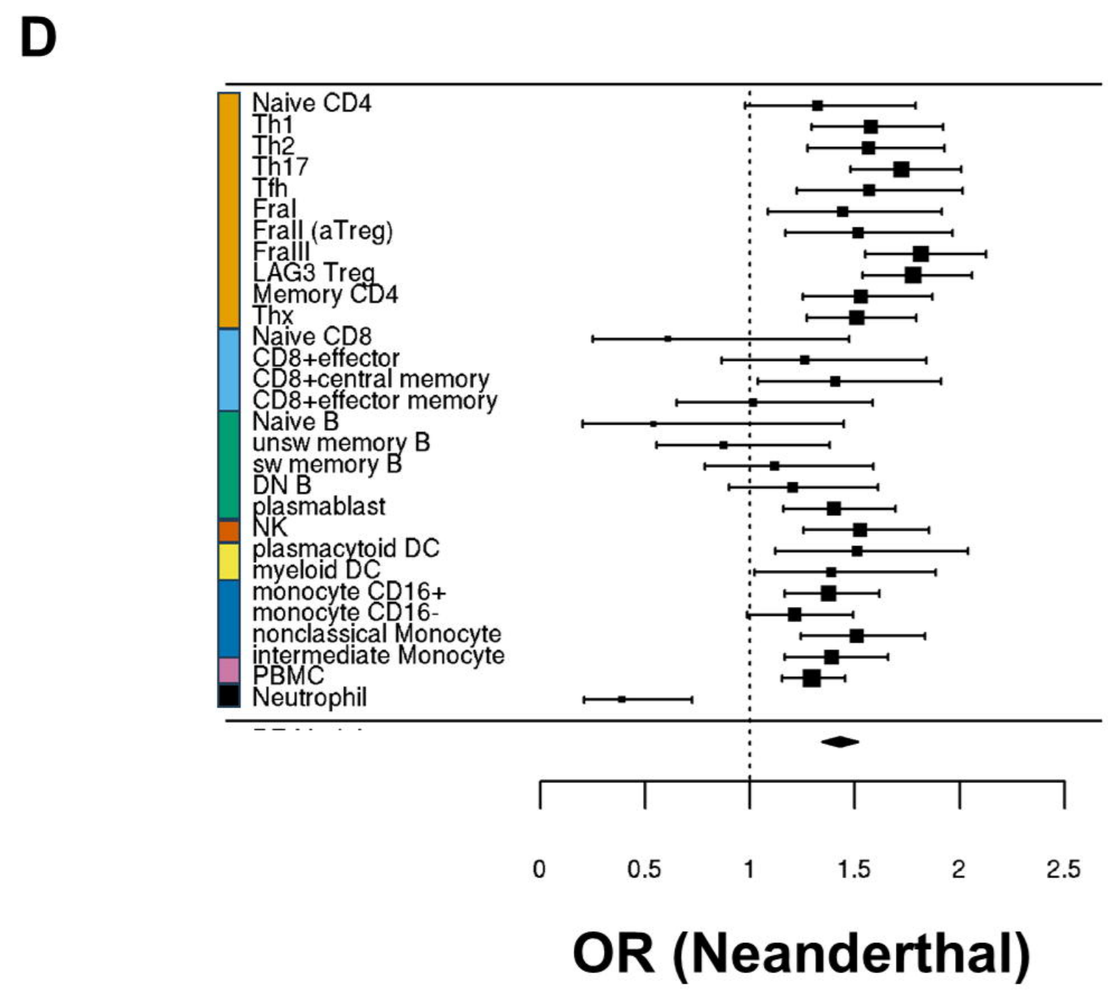

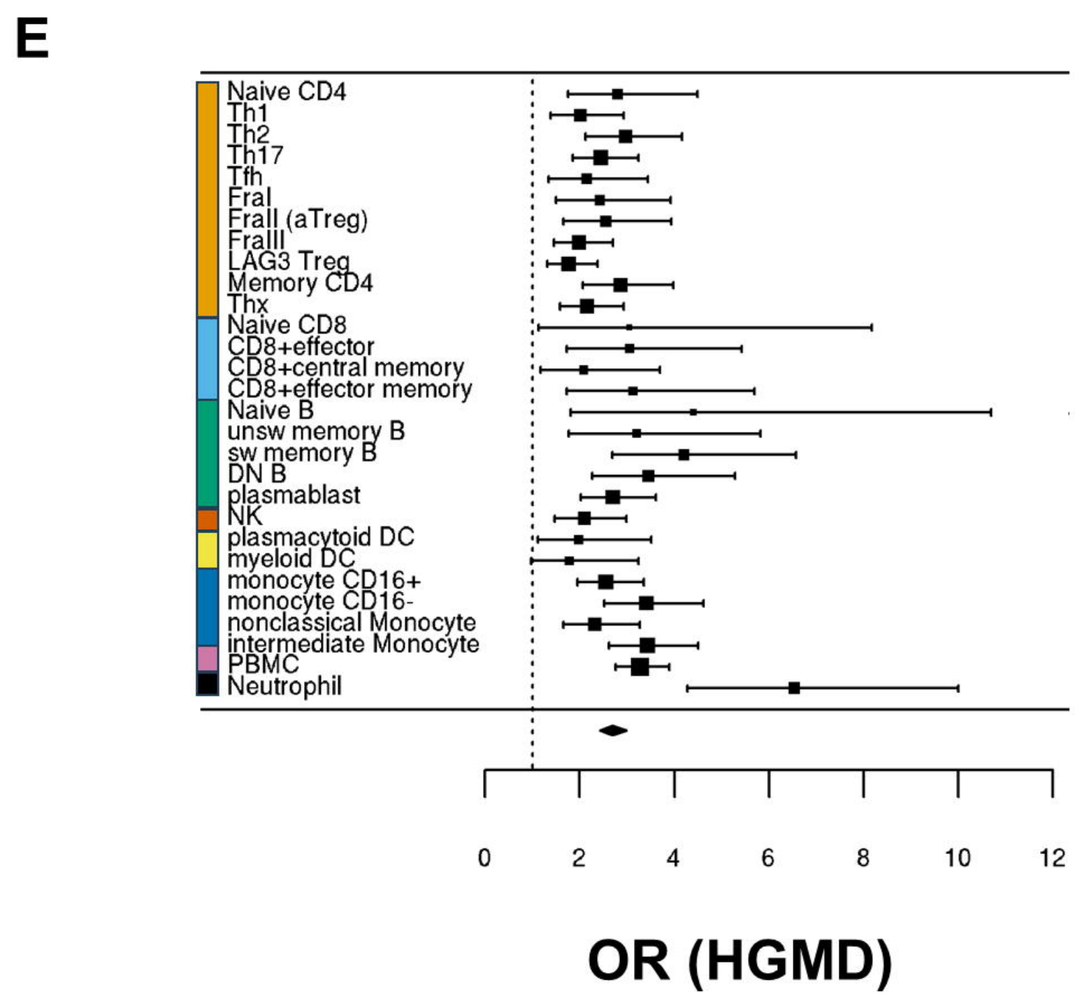

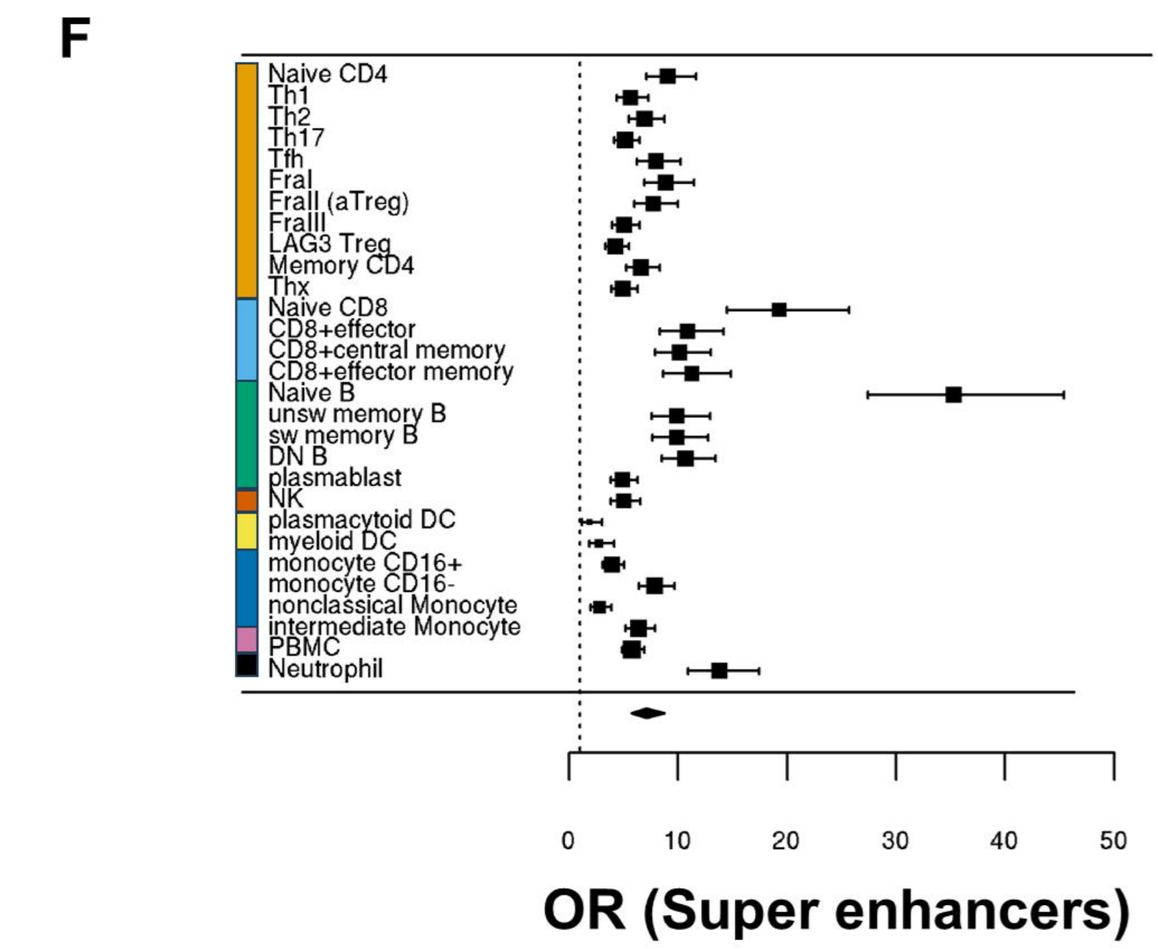

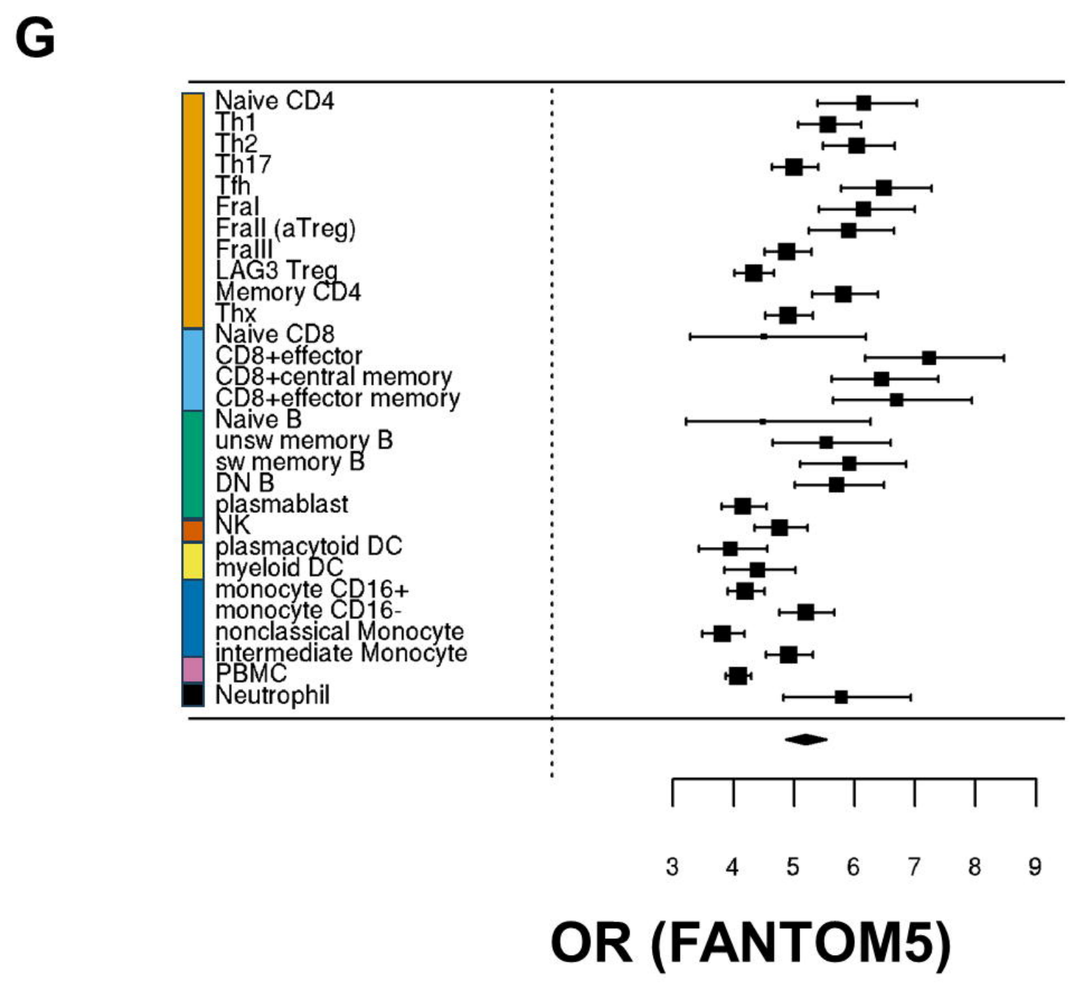

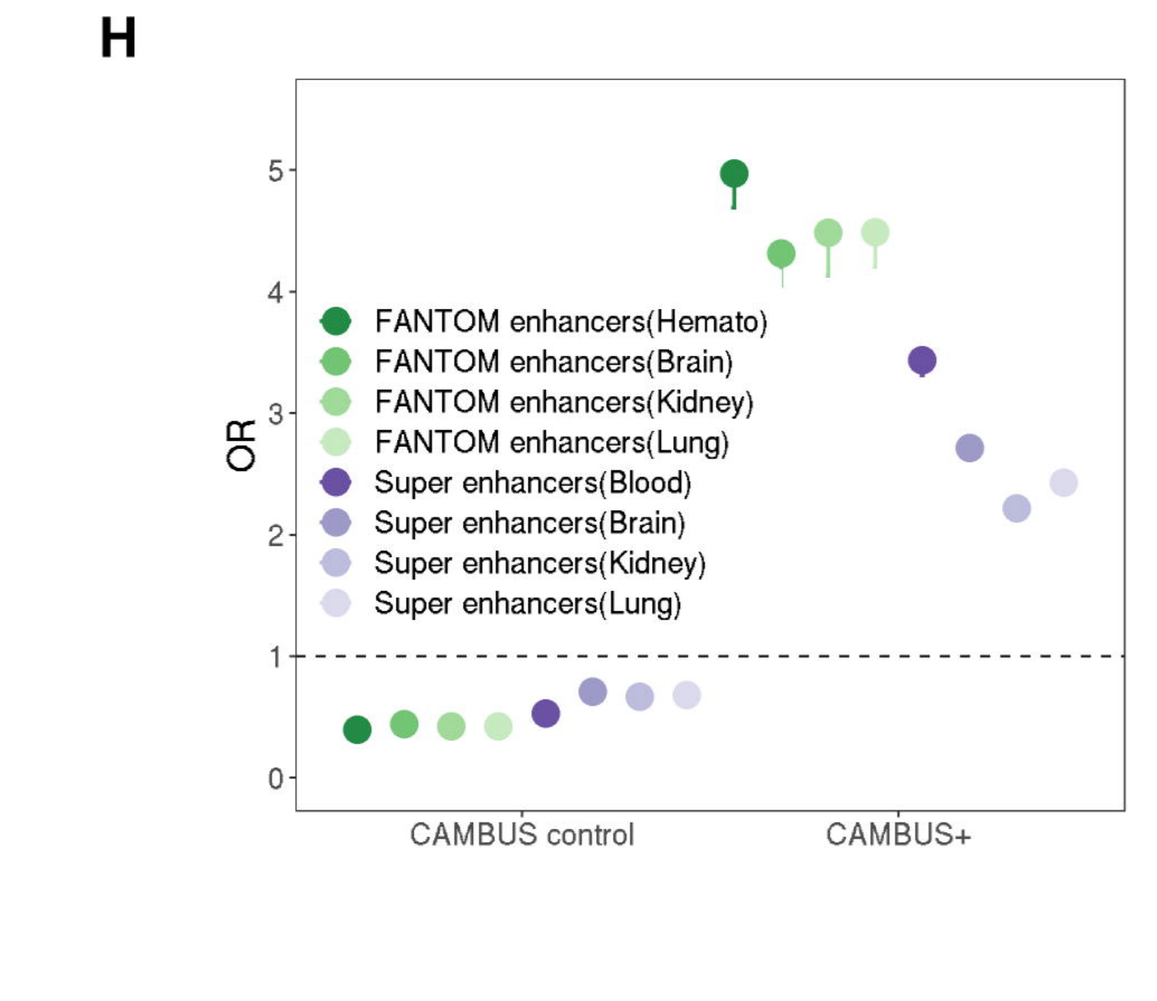

Figure S5 | Heritability enrichment for SLE EAS GWAS

A

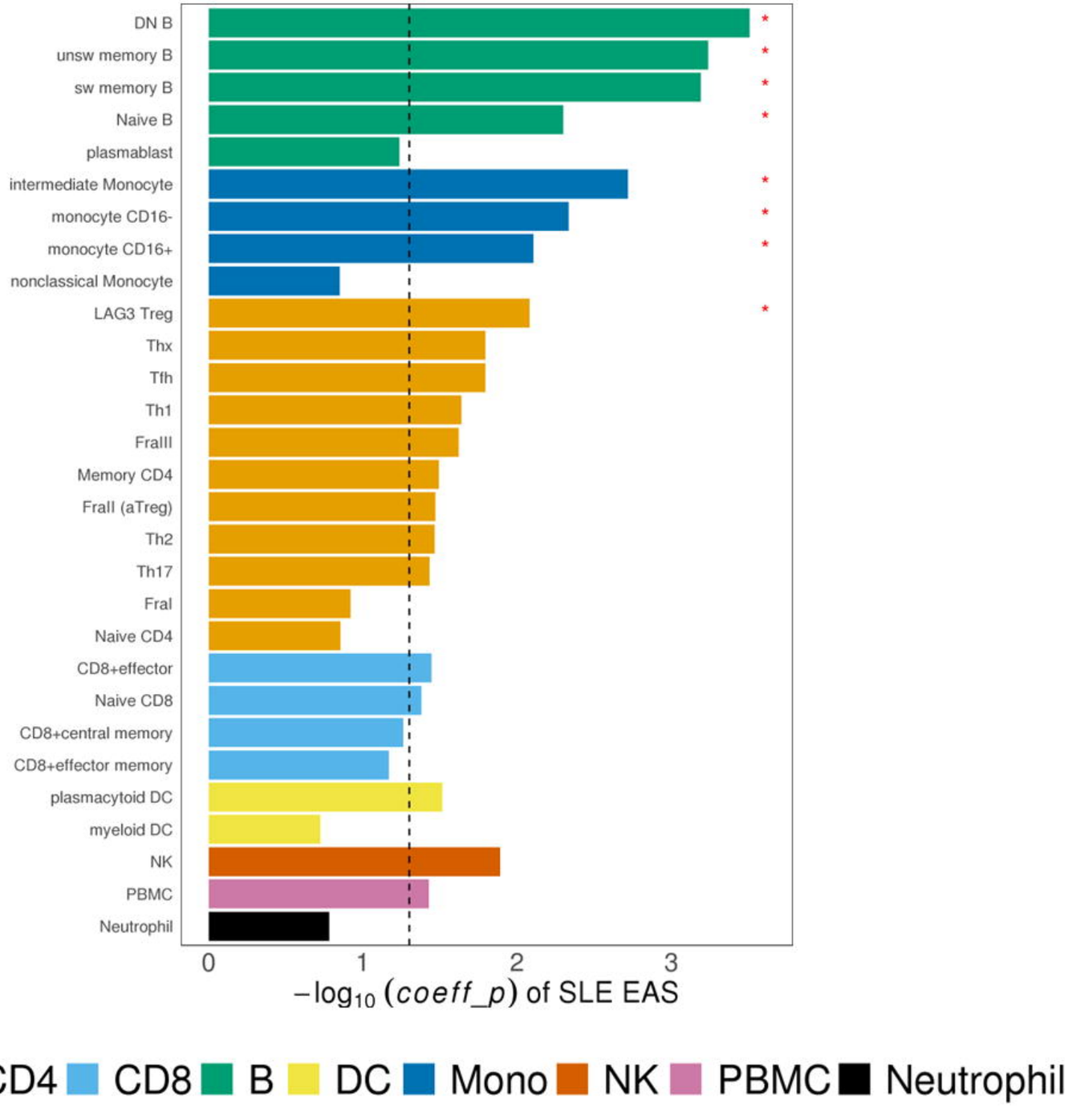

Figure S6 | Enrichment analysis for fine-mapped variants in CAMBUS+ OCRs

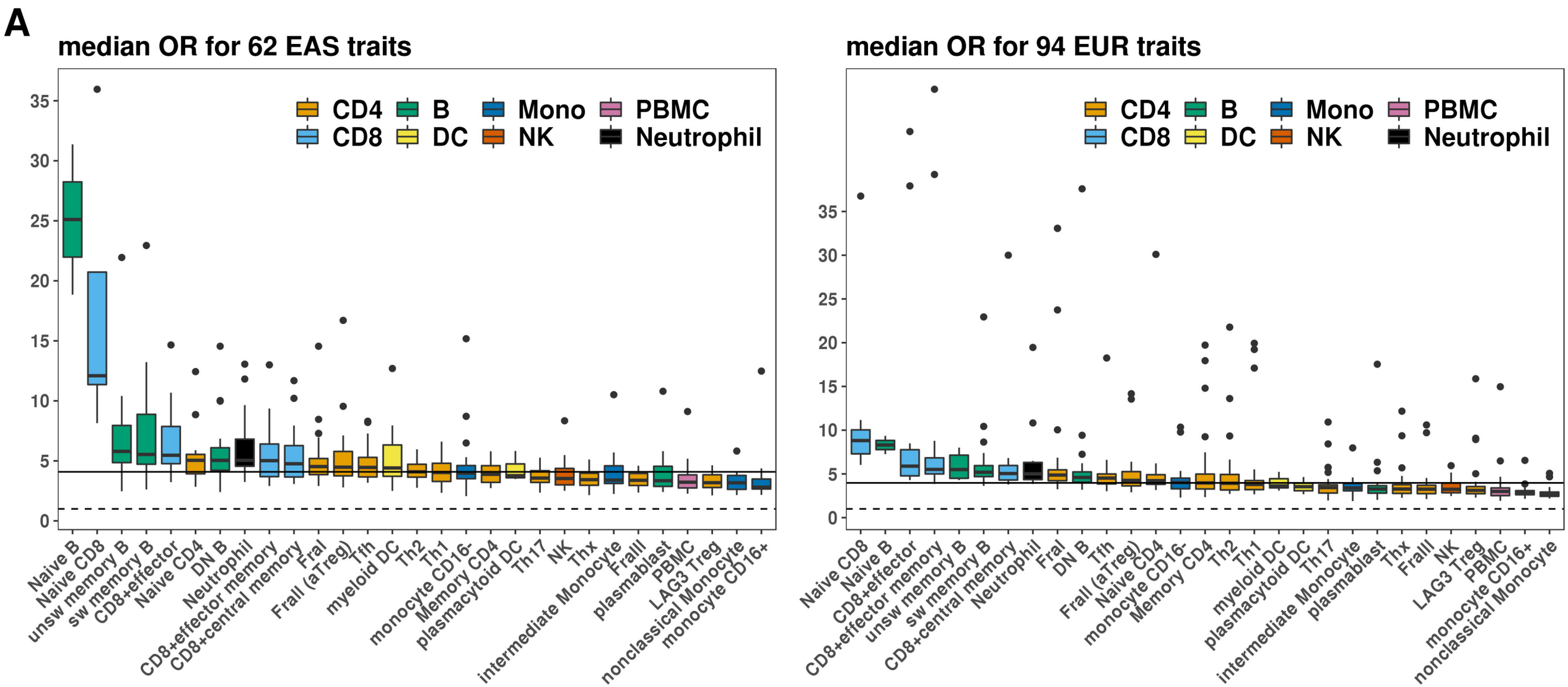

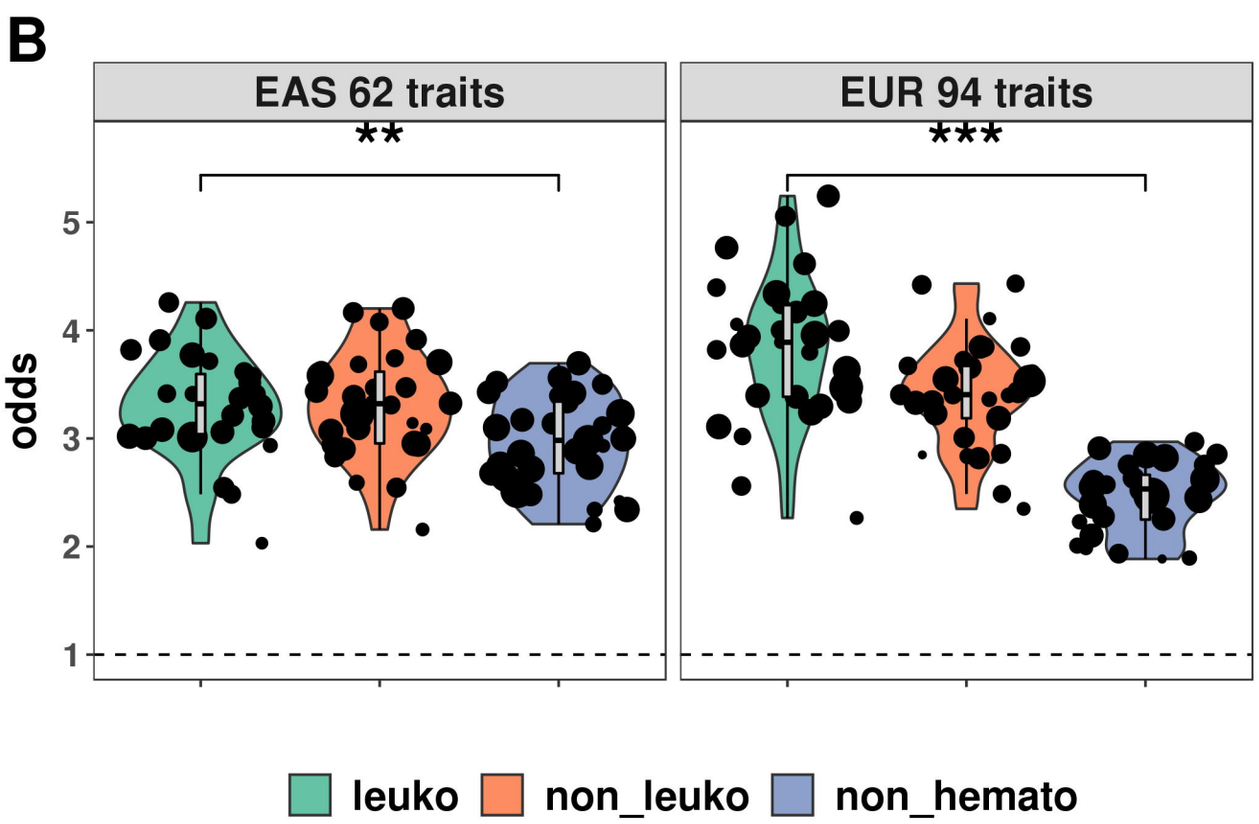
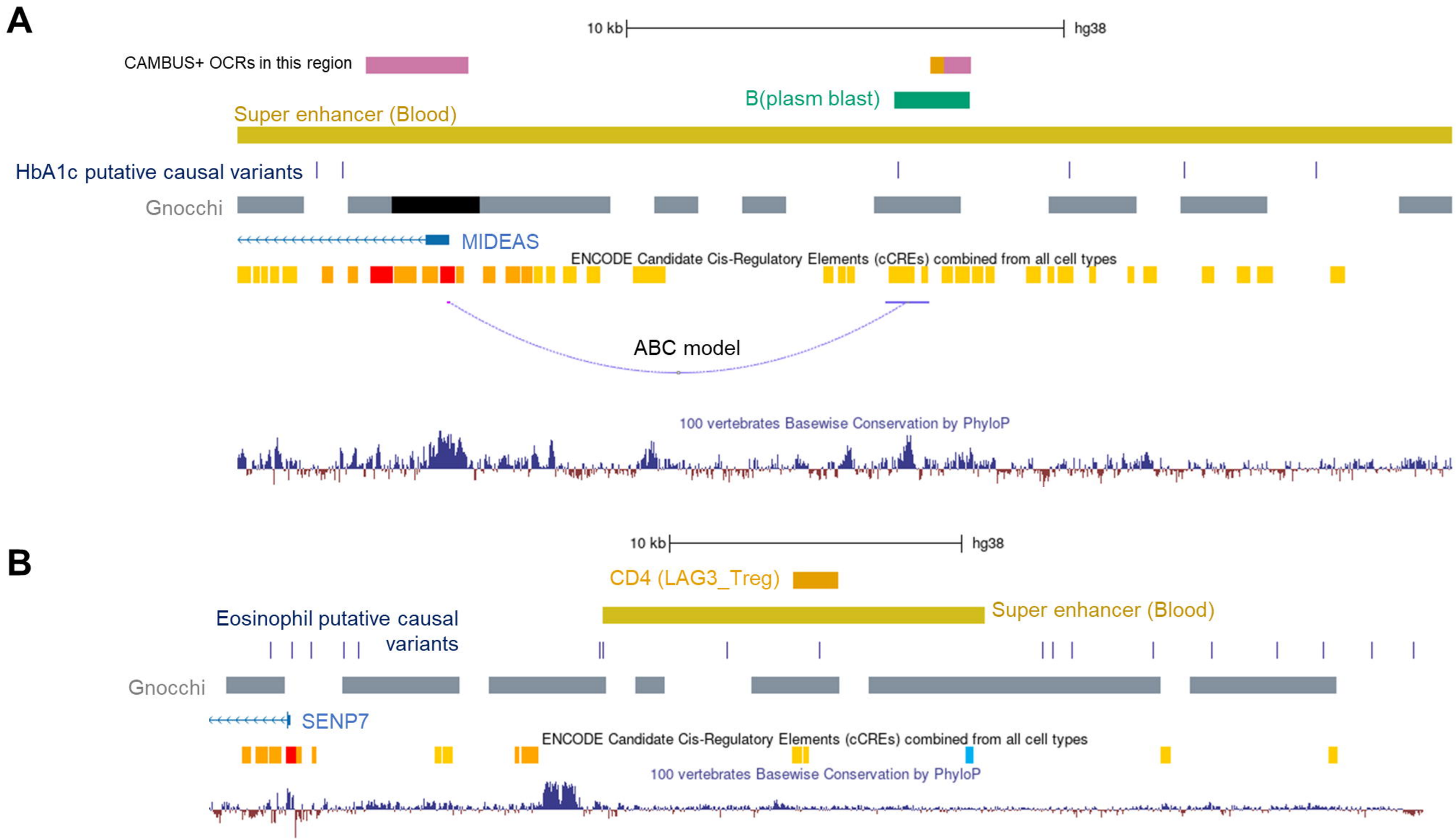
Figure S7 | Prioritization of the putative causal variants using CAMBUS+ OCRs